NASA Contractor Report 181911
ICASE Report No. 89–66

ICASE

LINEAR INSTABILITY OF SUPERSONIC PLANE WAKES

D. T. Papageorgiou

Contract No. NAS1–18605
September 1989

Institute for Computer Applications in Science and Engineering
NASA Langley Research Center
Hampton, Virginia 23665–5225

Operated by the Universities Space Research Association

National Aeronautics and
Space Administration

Langley Research Center
Hampton, Virginia 23665-5225

Linear instability of supersonic plane wakes.

D.T.Papageorgiou

The Levich Institute
City College of the City University of New York
Convent Avenue at 140th Street
New York, NY 10031

ABSTRACT

In this paper we present a theoretical and numerical study of the growth of linear disturbances in the high-Reynolds-number laminar compressible wake behind a flat plate which is aligned with a uniform stream. No ad hoc assumptions are made as to the nature of the undisturbed flow (in contrast to previous investigations) but instead the theory is developed rationally by use of proper wake-profiles which satisfy the steady equations of motion. The initial growth of near wake perturbations is governed by the compressible Rayleigh equation which is studied analytically for long- and short-waves. These solutions emphasize the asymptotic structures involved and provide a rational basis for a nonlinear development. The evolution of arbitrary wavelength perturbations is addressed numerically and spatial stability solutions are presented that account for the relative importance of the different physical mechanisms present, such as three-dimensionality, increasing Mach numbers and the non-parallel nature of the mean flow. Our findings indicate that for low enough (subsonic) Mach numbers, there exists a region of absolute instability very close to the trailing-edge with the majority of the wake being convectively unstable. At higher Mach numbers (but still not large - hypersonic) the absolute instability region seems to disappear and the maximum available growth-rates decrease considerably. Three-dimensional perturbations provide the highest spatial growth-rates.

[1]This research was supported by the National Aeronautics and Space Administration under NASA Contract No. NAS1-18605 while the author was in residence at the Institute for Computer Applications in Science and Engineering (ICASE), NASA Langley Research Center, Hampton, VA 23665.

1. Introduction.

In recent years there has been an increased interest in compressible shear layer flows due to the need in development of hypersonic propulsion systems for trans-atmospheric flight. The major problem that faces these projects, is the degree of stabilization that compressible mixing layers exhibit as the Mach number increases. This in turn means that the high degree of mixing that is desirable before ignition (in the scram-jet engine for example) is not available inside the system. A quantitative understanding of the instability mechanisms present is of much value, therefore. Some techniques have been suggested to alleviate this problem, by Kumar et al. (1987).

Most of the effort in understanding the stability of shear layers has been centered around the fully developed monotonic compressible shear layer which is typically modeled by a hyperbolic tangent distribution, together with the corresponding temperature profile (see for example Gropengiesser (1969), Jackson and Grosch (1989a,b), Ragab and Wu (1988)). In practical applications, such as those sited above, the mixing occurs when two streams come together at the trailing edge of a splitter plate to form a wake. If the free-stream velocities of the two components are different (usually this is the case, but in many cases they are numerically close) the tanh shear layer forms the far wake development of the steady equations of motion. There is a region closer to the trailing edge, where the unperturbed flow has a definite wake component. It is the purpose of this paper to analyze the instability mechanisms of this wake region. In order to fix matters we will consider the case of a plane wake where the free-stream values of the two oncoming fluid components are equal.

Incompressible wakes have been studied extensively for the existence of unstable waves through numerical and analytical solutions of the classical Rayleigh stability equation. Most early studies assume an ad hoc basic flow in the form of a gaussian or sech^2 velocity distribution (Hollingdale (1940); McKoen (1957); Sato and Kuriki (1961); Mattingly and Criminale (1972)). It is clear that such basic flow does not satisfy the equations of motion and at best provides the correct characteristics of the far-wake. Further more, the flow characteristics in the near wake are fairly complicated and involve the double structure described in the seminal work of Goldstein (1930), where there is a displaced outer boundary-layer region together with a thinner region including the wake center-line through which the abrupt change of boundary conditions (from no-slip upstream, to symmetry downstream) is accommodated. Papageorgiou and Smith (1989) (referred to as PS1) have considered incompressible

wake-stability, both analytically and numerically, using a correct basic flow that satisfies the equations of motion for large Reynolds numbers (the wake-boundary-layer equations of Goldstein). The non-linear development of the instability is analyzed in an accompanying paper, Papageorgiou and Smith (1988) (referred to as PS2).

A very interesting and physically important aspect of shear layer flows is the possibility of convective or absolute instabilities. For an account of the ideas involved in shear layer stability see Huerre and Monkewitz (1985), Huerre (1987). This aspect of instability has been studied by Betchov and Criminale (1966) and more recently by Hultgren and Aggarwal (1987), for a two-parameter family of model basic states. More specifically the basic flow is assumed to have the form $\bar{u} = 1 - a\, e^{-by^2}$, where $0 \le a \le 1$, $b > 0$ or an equivalent sech^2 distribution. Hultgren and Aggarwal for example, find that the flow becomes absolutely unstable when $a \ge 0.943$. Such a profile clearly corresponds to a station very close to the trailing edge as we briefly demonstrate. The center-line velocity of the proposed absolute-instability profiles is at most 0.057 in non-dimensional terms. Using Goldstein's results (see also Smith (1984)) we know that the velocity in the near-wake at the center-line is given by $1.611x^{1/3}\lambda^{2/3}$ where λ is the Blasius skin-friction and is equal to 0.33206... . Equating the value 0.057 with this, gives the value for the non-dimensional x-station to be $x = 0.0004017$, or $\xi = x^{1/3} = 0.0738$. The basic flow at this point does not seem to be representable by the gaussian model (see our results section) and so some serious objections may be raised as to the rational prediction of convective/absolute change-overs by use of such models. The trends seem to be correct, however, in comparison to the results of PS1 which suggest an absolute instability region very near the trailing edge. The important question that arises in supersonic wakes is, besides the possibility of absolute instability regions per se, the characteristics of an absolute instability region as the Mach number increases. This is addressed numerically for two Mach numbers that are representative of the different physics that is involved; these are 0.1 and 3.0 corresponding to compressible subsonic and supersonic flow respectively. It is found that the subsonic flow contains a region of absolute instability whereas the supersonic one seems not to. The streamwise station at which the change-over from convective to absolute instability takes place for M=0.1 is less than 0.000001 in non-dimensional terms.

The purpose of the present work is to extend the incompressible study of PS1 to compressible flows of arbitrary Mach numbers. Our approach is that of classical linear stability theory that covers both two- and three-dimensional disturbances. In Section 2 we briefly describe the basic flow and

formulate the linear stability problem that leads to the compressible Rayleigh equation. Section 3 is used to analyze the stability of short-wave disturbances in the very near wake where the compressible analogue of the Goldstein double structure provides an asymptotic description for the unperturbed flow. In Section 4 we consider the behavior of long-waves (these waves are long compared to the boundary-layer thickness but not as long as the plate length-see Section 2 also). Section 5 discusses numerical solutions of the Rayleigh equation using the nominally exact unperturbed profiles that are in turn computed numerically. In Section 6 we present numerical results for a range of streamwise stations, Mach numbers and angles of wave propagation, and finally we draw some conclusions.

Throughout the paper we use a cartesian frame of coordinates which is fixed at the trailing edge $x = 0$. The flow quantities ρ , u , v , w , p , T , μ denote non-dimensional density, velocities in the x, y and z directions, pressure, temperature and viscosity coefficient respectively, where non-dimensionalizations are made with respect to free-stream values which are denoted by a subscript ∞. The Reynolds number is $R_e = \dfrac{U_\infty L}{\nu_\infty}$ where L is the plate length, the Mach number is $M = U_\infty/a$ where a is the sound-speed and the Prandtl number is $Pr = \mu_\infty c_p/k$ where c_p is the specific heat at constant pressure and k is the coefficient of thermal diffusivity. R_e is taken to be asymptotically large throughout, while M_∞ is arbitrary within the context of validity of the equations of motion. The governing equations used are the 2D steady and pressure-free (classical) compressible boundary-layer equations for the calculation of the basic flow (bars are used to distinguish the basic flow), or the unsteady compressible 3D Euler equations for the evolution of wavy disturbances. We give these here for future reference.

$$\bar{\rho} (\bar{u} \bar{u}_x + \bar{v} \bar{u}_y) = (\bar{\mu} \bar{u}_y)_y \quad , \tag{1.1a}$$

$$\bar{\rho} (\bar{u} \bar{T}_x + \bar{v} \bar{T}_y) = \frac{1}{Pr} (\bar{\mu} \bar{T}_y)_y + (\gamma - 1) M^2 \bar{\mu} \bar{u}_y^2 \quad , \tag{1.1b}$$

$$(\bar{\rho} \bar{u})_x + (\bar{\rho} \bar{v})_y = 0 \quad , \tag{1.1c}$$

$$\bar{\rho} \bar{T} = 1 \quad . \tag{1.1d}$$

The boundary conditions are

$$\bar{u}_y (x , 0) = \bar{T}_y (x , 0) = 0 \quad , \quad \bar{u}(x,\infty) = \bar{T}(x,\infty) = 1 \quad . \tag{1.1BC}$$

The 3D Euler equations are used in the form

$$\rho\,(u_t + u\,u_x + v\,u_y + w\,u_z) = -\frac{1}{\gamma M^2}\,p_x \quad , \tag{1.2a}$$

$$\rho\,(v_t + u\,v_x + v\,v_y + w\,v_z) = -\frac{1}{\gamma M^2}\,p_y \quad , \tag{1.2b}$$

$$\rho\,(w_t + u\,w_x + v\,w_y + w\,w_z) = -\frac{1}{\gamma M^2}\,p_z \quad , \tag{1.2c}$$

$$\rho\,(T_t + u\,T_x + v\,T_y + w\,T_z) = \frac{1}{\gamma M^2}\,(p_t + u\,p_x + v\,p_y + w\,p_z) \quad , \tag{1.2d}$$

$$\rho_t + (\rho\,u)_x + (\rho\,v)_y + (\rho\,w)_z = 0 \quad , \tag{1.2e}$$

$$p = \rho\,T\,(\gamma - 1)\,M^2 \quad . \tag{1.2f}$$

2. Basic flow and formulation of the linear stability problem.

The formulation that leads to the compressible Rayleigh equation essentially follows that of the incompressible analogue, as described in PS1 for example. It is instructive, however, to bear in mind the scales for which the Rayleigh equation is valid in the case of a planar wake. The arguments of PS1 carry over to the present problem also (the important physical mechanism is the asymptotically large Reynolds number which is common to both flows), and the instability develops on a local region of horizontal and lateral extent of order $R_e^{-1/2}$; the time scale of the instability is also of order $R_e^{-1/2}$. These scalings insure the inviscid development of wavy disturbances of the viscous underlying basic flow. Further more, as is usual in Rayleigh-type evolutions, the scales are such that the x-variation of the basic flow as well as its lateral component, are higher order effects. In the present problem the streamwise component of the basic flow varies on an order one x-scale while the lateral component is of order $R_e^{-1/2}$. Viscosity becomes important when the wavelength of the perturbation becomes of order unity as compared to the wake-thickness. For more details of the scaling analysis see PS1 and PS2.

Before the introduction of a perturbation it is useful to summarize the characteristics of the underlying unperturbed state. This is described in detail by Papageorgiou (1989) and we sketch the results here. The governing equations are (1.1a-d) together with the boundary conditions (1.1BC). Next we assume a model fluid and a linear viscosity law, i.e. the Prandtl number $Pr = 1$ and $\mu = C\,T$ (Chapman's law, C is a constant that is scaled out of the problem and the equation $\mu = T$ is used).

The Dorodnitsyn-Howarth transformation $Y = \int_0^y \frac{dy}{T}$ is employed, from which it is seen that Crocco's equation (see Stewartson (1964)) becomes

$$\frac{\partial^2 \overline{T}}{\partial \overline{u}^2} = -(\gamma - 1) M^2 \quad .$$

It follows that $\overline{T}$ involves two constants of integration which can be found by matching with the upstream flow. Two physically distinct cases are given, (i) constant wall temperature, T_w say, on the plate, and (ii) insulated walls (i.e. the temperature gradient is zero on the plate upstream). In case (i) the result is

$$\overline{T}(x , Y) = 1 + \frac{1}{2} (\gamma - 1) M^2 (\overline{u} - \overline{u}^2) + (T_w - 1) (1 - \overline{u}) \quad , \tag{2.1}$$

while in case (ii) we have

$$\overline{T}(x , Y) = 1 + \frac{1}{2} (\gamma - 1) M^2 (1 - \overline{u}^2) \quad . \tag{2.2}$$

In order to solve for the velocity $\overline{u}(x,Y)$, conditions must also be given at the outset $x = 0$ since the problem is parabolic in x. The nonlinear system that gives the undisturbed flow is

$$\overline{u} = \overline{\psi}_Y \quad , \quad \overline{u}\, \overline{u}_x - \overline{\psi}_x\, \overline{u}_Y = \overline{u}_{YY} \quad , \tag{2.3}$$

holding for $x > 0$, together with the boundary conditions

$$\overline{u}(x , \infty) = 1 \quad , \quad \overline{\psi}(x , 0) = \overline{u}_Y(x , 0) = 0 \quad , \quad \overline{\psi}(0+ , Y) = \psi_B(Y) \quad , \tag{2.3BC}$$

where ψ_B' represents the Blasius velocity profile given by

$$\psi_B''' + \frac{1}{2} \psi_B \psi_B'' = 0 \quad , \quad \psi_{B(0)} = \psi_B'(0) = \psi_B'(\infty) - 1 = 0 \ ; \ \psi_B''(0) = \lambda = 0.332... \quad .$$

We will be mainly concerned with adiabatic wall conditions but the results can be extended to constant wall temperatures also.

With the basic flow assumed known, a perturbation of size ε_1 is introduced so that the total flow has the form

$$(u , v , w , \rho , T , p) = (\overline{u} , 0 , 0 , \overline{\rho} , \overline{T} , 0) + \varepsilon_1 (\tilde{u} , \tilde{\phi} , \tilde{w} , \tilde{\rho} , \tilde{T} , \tilde{p}) e^{i (\alpha x + \beta z - \omega t)} \quad ,$$

where the tilde functions depend on y alone. Substitution into (1.2a-f) (we are anticipating the inviscid

result here; equivalently a substitution into the Navier-Stokes equations together with the instability scales described earlier yields the same result), and linearization with respect to ε provides a linear system of five ordinary differential equations. We will work with the transformed variable Y rather than the physical one and will use the following forms of the compressible Rayleigh equation obtained by elimination of four unknowns and dropping of the tildes :

$$p'' - \frac{2\bar{u}'}{\bar{u} - c}\, p' - \bar{T}^2 \left[\alpha^2 + \beta^2 - \frac{\alpha^2}{\bar{T}} (\bar{u} - c)^2 M^2 \right] p = 0 \quad , \tag{2.4}$$

$$\frac{d}{dY} \left[\frac{(\bar{u} - c) \phi' - \bar{u}' \phi}{G \bar{T}} \right] - \alpha^2 (\bar{u} - c) \phi = 0 \quad , \tag{2.5}$$

where primes denote Y-derivatives and G is given by

$$G = \frac{\alpha^2 + \beta^2}{\alpha^2} \bar{T} - M^2 (\bar{u} - c)^2 \quad .$$

Equations (2.4) and (2.5) describe the evolution of perturbation pressure and normal velocity respectively; (2.5) was used by Gropengiesser (1969) in his study of shear layers. There is a choice in boundary conditions at the wake center-line Y = 0, due to the symmetry of the basic flow. We choose to study two distinct wake-modes, anti-symmetric ones (mode I) and symmetric ones (mode II). The convention used here is that of incompressible wake stability whereby the perturbation is termed anti-symmetric/symmetric if the streamwise velocity perturbation, u, is anti-symmetric/symmetric with respect to Y=0. It is generally found that the anti-symmetric ones are the most dangerous ones. Experimental evidence lends weight to this finding through the well-known Karman vortex-street found in wakes. The boundary conditions used are, therefore,

$$\text{Mode I} \quad p(Y=0) = 0 \quad , \quad p(Y=\infty) = 0 \quad , \quad \text{Mode II} \quad p'(Y=0) = 0 \quad , \quad p(Y=\infty) = 0 \quad , \tag{2.4BC}$$

$$\text{Mode I} \quad \phi'(Y=0) = 0 \quad , \quad \phi(Y=\infty) = 0 \quad , \quad \text{Mode II} \quad \phi(Y=0) = 0 \quad , \quad \phi(Y=\infty) = 0 \quad . \tag{2.5BC}$$

Here we have assumed that the disturbance decays at infinity. This assumption is reasonable since, in contrast to shear layers, there does not exist a supersonic region that can support neutrally stable oscillatory outgoing waves (see comments of Section 6 also; for a discussion of supersonic shear waves see Jackson and Grosch (1989a)). The eigenvalue problems defined by (2.4), (2.4BC) or (2.5), (2.5BC) are equivalent and must, in general, be addressed numerically. This is done in Section 5, but before discussing numerical solutions we consider two important limits which are amenable to analysis. These

limits are short- and long-waves which in 2D temporal theory are characterized by $\alpha \to \infty$ and $\alpha \to 0$ respectively (see PS1). It is worth noting that short- and long-wave analyses only make sense for temporal theories, but as it turns out the growth rates are asymptotically small in both cases thereby making the results readily applicable to spatial stability via the Gaster (1968) group velocity transformation. The analysis of the following sections considers two-dimensional waves and these results are extendible to three-dimensional ones after minor modifications.

3. Short waves, $\alpha \to \infty$.

In this section we construct the asymptotic behavior of the solutions in the limit of large α. The physical structure of these waves is that they have length-scales which are small compared to the wake thickness. Further more we concentrate on the near-wake where the basic flow is described by the Goldstein double structure (see Papageorgiou (1989) for example). Our analysis can be viewed in terms of the double limit $x \to 0$ and $\alpha \to \infty$. The ideas and structures involved are similar to the incompressible case studied in PS1, but the growth rates we compute here are larger than their incompressible counterparts.

The starting point is the Rayleigh equation (2.5) which is considered for 2D anti-symmetric (mode I) disturbances - equivalently the pressure equation can be used, as well as mode II waves but as the subsequent numerical results indicate, mode I waves are more unstable (see comments in the introduction also). Inspection suggests the following expansions in the re-scaled region $Y = \alpha^{-1}\,\eta$ with $\eta = O(1)$:

$$\phi = \phi_0 + \alpha^{-1}\,\phi_1 + \alpha^{-2}\,\phi_2 + \cdots \quad , \tag{3.1a}$$

$$\bar{u} = \pm\,\alpha^{-1}\,\lambda\,\eta + \alpha^{-4}\,\lambda_4\,\eta^4 + \cdots \quad , \tag{3.1b}$$

$$c = c_0 + \alpha^{-1}\,c_1 + \alpha^{-2}\,c_2 + \alpha^{-3}\,c_3 + \cdots \quad . \tag{3.1c}$$

For adiabatic walls the temperature expands as

$$\bar{T} = T_0 - \alpha^{-2}\,\eta^2\,T_2 + \cdots \quad , \quad T_0 = 1 + \frac{1}{2}(\gamma-1)M^2 \quad , \quad T_2 = \frac{1}{2}(\gamma-1)\lambda^2 M^2 \tag{3.1d}$$

The constant λ in (3.1b) is the skin-friction of the Blasius flow discussed in the previous section, and $\lambda_4 = -(1/48)\,\lambda^2$. The expansion (3.1b) reflects the fact that we are outside the Goldstein layer where

the basic flow is essentially the displaced Blasius flow. In the analysis that follows the Goldstein layer (of thickness $x^{1/3}$) is thin compared to the wavelength $2\pi/\alpha$; the ordering $\alpha^{-1} \gg x^{1/3}$ is therefore observed. Physically this corresponds to the development of waves which are short compared to the boundary-layer thickness but not as short as the Goldstein layer thickness. It can also be seen that given any large α , the position x can be chosen to be small enough so as to validate the above ordering (this is achievable as long as $x \gg R_e^{-3/8}$ which means that we are still outside the triple-deck).

In view of the above, the Goldstein layer can be regarded as a sharp interface across which the perturbation pressure and normal velocity must be continuous. This means that the following conditions hold to all orders in α^{-1} :

$$[\ \phi\ ] = 0 \quad , \quad [\ (\ \bar{u} - c\ )\ \phi_\eta - \bar{u}'\ \phi\ ] = 0 \quad , \tag{3.2a,b}$$

where the square bracket denotes the jump across $\eta = 0$. In view of these physical constraints, we find that for a non-trivial solution the leading order phase-speed vanishes, i.e.

$$c_0 = 0 \quad .$$

is not surprising in view of the fact that the basic flow has a maximum streamwise component of α^{-1} with which it can convect disturbances downstream. Substitution of (3.1a-d) into (2.5) gives llowing solution to leading order

$$\phi_0^{\pm} = A_0\, e^{-\ +\ T_0\,\eta} \quad , \tag{3.3}$$

$\pm$ refers to the solution for $\eta > 0$ and $\eta < 0$ respectively. Condition (3.2a) has been used to ıe same constant A_0 in the upper and lower half planes respectively. When the leading order n (3.3) is used in the pressure continuity condition (3.2b), and $O(\alpha^{-1})$ are balanced, we obtain ding contribution to the phase-speed to be

$$c_1 = \frac{\lambda}{T_0} \quad , \tag{3.4}$$

the compressible analogue of the result in PS1. It can be seen from this expression that the eed of the perturbation decreases with increasing Mach number (cf. (3.1d)) and in fact decays cally in the hypersonic limit. Next we find $\phi_2 = 0$, $c_2 = 0$ (see below). This implies that the ves constructed here are almost neutral and have growth-rates of $O(\alpha^{-3})$ at most. This is in to the incompressible problem which yields $O(\alpha^{-4})$ growth-rates (cf. PS1). The complex

coefficient c_3 is computed by construction of uniformly valid asymptotic expansions which are matched across the critical layers and the central Goldstein layer to satisfy the boundary conditions and so provide the correction to the eigenvalue problem.

Before proceeding to the higher order approximations, it is useful to introduce a new vertical coordinate ξ, given by $\xi = T_0 \eta$; this simplifies the algebraic expressions since the critical layers now occur at $\xi = \pm 1$ (see below). The next corrections to the eigenfunction satisfy the following equations, then

$$(\pm \xi - 1) (\phi_{1\xi\xi} - \phi_1) = 0 \quad , \quad \phi_1(\pm\infty) = 0 \quad , \tag{3.5}$$

$$\phi_{2\xi\xi} - \phi_2 = \pm 2 S (\gamma \xi + 1) e^{+\xi} - S(\gamma\xi^2 + 2\xi + 1) e^{+\xi}$$

$$\pm \frac{2S ((\gamma-1)\xi + 1)}{(\pm\xi - 1)} e^{+\xi} \quad , \quad \phi_2(\pm\infty) = 0 \quad , \tag{3.6}$$

where as before the upper sign is to be taken in the region $\xi > 0$ and the lower one in $\xi < 0$. The constant S appearing in 3.6 is given by

$$S = \frac{\lambda^2 A_0 M^2}{T_0^3} \quad .$$

The solution for ϕ_1 is identical to that of ϕ_0 and so, without loss of generality, it is taken to be zero by re-normalization of A_0. As mentioned earlier, it can be seen that (3.6) has singularities at the levels $\xi = \pm 1$; these singularities are critical layers and arise because the phase-speed is neutral to leading order (cf. (3.4) above). The solution for ϕ_2 then splits up into four distinct regions (cf. Figure 1 in PS1). The four regions $1 < \xi < \infty$, $0 < \xi < 1$, $-1 < \xi < 0$, $-\infty < \xi < -1$ are denoted by (1), (2), (3) and (4) respectively and the following solutions are found

$$\phi_2^{(1)} = e^{-\xi} [B_1 - S (-\frac{1}{6}\gamma\xi^3 + \frac{1}{2} (\gamma+1) \xi^2 + (\gamma-\frac{3}{2}) \xi + (\gamma-2) \ln(\xi - 1)$$

$$+ S e^{\xi} \int_{\infty}^{\xi} [-\frac{1}{2}\gamma\xi_1^2 + (\gamma+1) \xi_1 + (\gamma-\frac{3}{2}) + \frac{(\gamma-2)}{\xi_1-1}] e^{-2\xi_1} d\xi_1 \quad , \tag{3.7a}$$

$$\phi_2^{(2)} = e^{-\xi} [B_2 - S (-\frac{1}{6}\gamma\xi^3 + \frac{1}{2} (\gamma+1) \xi^2 + (\gamma-\frac{3}{2}) \xi + (\gamma-2) \ln|\xi - 1|$$

$$+ A_2 e^{\xi} + S e^{\xi} \int_{0}^{\xi} [-\frac{1}{2}\gamma\xi_1^2 + (\gamma+1) \xi_1 + (\gamma-\frac{3}{2}) + \frac{(\gamma-2)}{\xi_1-1}] e^{-2\xi_1} d\xi_1 \quad , \tag{3.7b}$$

$$\phi_2^{(3)} = e^{\xi} \left[B_3 + S \left(-\frac{1}{6}\gamma\xi^3 - \frac{1}{2}(\gamma+1)\xi^2 + (\gamma-\frac{3}{2})\xi - (\gamma-2)\ln(\xi+1)\right.\right.$$

$$\left.\left. + A_3 e^{-\xi} - S e^{-\xi} \int_0^{\xi} \left[-\frac{1}{2}\gamma\xi_1^2 - (\gamma+1)\xi_1 + (\gamma-\frac{3}{2}) - \frac{(\gamma-2)}{\xi_1+1} \right] e^{2\xi_1} d\xi_1 \right. \right] , \qquad (3.7c)$$

$$\phi_2^{(4)} = e^{\xi} \left[B_4 + S \left(-\frac{1}{6}\gamma\xi^3 - \frac{1}{2}(\gamma+1)\xi^2 + (\gamma-\frac{3}{2})\xi - (\gamma-2)\ln|\xi+1|\right.\right.$$

$$\left.\left. - S e^{-\xi} \int_{-\infty}^{\xi} \left[-\frac{1}{2}\gamma\xi_1^2 - (\gamma+1)\xi_1 + (\gamma-\frac{3}{2}) - \frac{(\gamma-2)}{\xi_1+1} \right] e^{2\xi_1} d\xi_1 \right. \right] , \qquad (3.7d)$$

In matching solutions across the critical levels we assume that the constants in the various regions are suitably connected so as to render our inviscid solution as the zero viscosity limit of the Orr-Sommerfeld equation. This amounts to picking up the correct branch from the complex logarithmic dependence as has been explained by Lin (1955), Lees and Lin (1946) (see also Drazin and Reid (1981)). The net effect, therefore, is a phase-jump of $-i\pi\ \mathrm{sgn}(\bar{u}'(\xi = \pm 1))$ as a critical level is crossed from above (the temperature basic state is passive in this because it is positive throughout the domain). Another set of connection equations is obtained from the continuity of ϕ across the levels $\xi = \pm 1$. The analysis is fairly lengthy so we just give the results here. The following four algebraic equations are obtained that connect the six unknowns A_1 , A_2 , B_1 , B_2 , B_3 , B_4 :

$$B_1 - B_2 - e^2 A_2 = e\,(p_3 - p_1) \quad , \qquad (3.8a)$$

$$B_1 - B_2 + e^2 A_2 = p_4 - 2\pi i S(\gamma-2) \quad , \qquad (3.8b)$$

$$B_3 - B_4 + e^2 A_3 = e\,(p_7 - p_5) \quad , \qquad (3.8c)$$

$$B_3 - B_4 - e^2 A_3 = -e\,(p_6 + p_8) + 2\pi i S(\gamma-2) \quad , \qquad (3.8d)$$

where p_1 , p_3 , p_4 , p_5 , p_6 , p_7 , p_8 are real constants that arise from the limiting values of individual solutions as the critical layers are approached from above or below. The exact effect of these constants is of secondary importance to our purpose here since they are real valued and do not contribute towards the instability. The complex terms (phase-jumps from the critical layers) are explicitly included in the equations (3.8a-d) above.

The remaining two algebraic equations that enable complete solution for ϕ_2 are obtained by consideration of the Goldstein layer dynamics. We point out again that the scales involved are essentially those of the incompressible problem of PS1; the compressibility effects, however, introduce

perturbation dynamics at a lower order. The Goldstein layer has thickness $\varepsilon = x^{1/3} \ll 1$. A rescaling of the Dorodnotsyn-Howarth variable is required, therefore, and the order one variable Z is introduced, given by $Y = \varepsilon Z$. Consideration of the outer solutions for small η (or ξ) suggests that the eigenfunction inside the Goldstein layer proceeds in powers of $\varepsilon\alpha$ (this comes from the expansion of ϕ_0). The next outer correction is $\alpha^{-2}\,\phi_2$ and as we have shown above ϕ_2 contains an order-one displacement. Further more it is clear that instability will arise from the contribution of ϕ_2 (it contains the complex phase-jumps) and so we chose to structure our expansion so that the effects of ϕ_2 come in at second order. This requires the balance $\varepsilon\alpha = \alpha^{-2}$ or $\varepsilon = \alpha^{-3}$. In view of the definition of ε this scaling implies an asymptotic wavelength of order $x^{1/12}$ as x tends to zero. The validity of the solutions can be improved by a double expansion in powers of α^{-1} and $\varepsilon\alpha$, whereby the asymptotic condition is $\varepsilon\alpha \ll 1$. Both methods give the same final result (as was found for the incompressible problem of PS1 also) and for brevity we present the former analysis.

Using α^{-1} as the perturbation parameter the Goldstein layer is given by $Y = \alpha^{-3} Z$ and the expansions are found to be

$$\phi_G(Z) = \Phi_0(Z) + \alpha^{-2}\Phi_1(Z) + \alpha^{-4}\Phi_2(Z) + \cdots \quad , \tag{3.9a}$$

$$\overline{u} = \alpha^{-3} F(Z) + O(\alpha^{-12}) \qquad F(Z) \sim \pm \lambda\,(|Z| + \Lambda_G) \ \text{ as } Z \to \pm\infty \quad , \tag{3.9b}$$

$$\overline{T} = T_0 - \frac{1}{2}\,\alpha^{-6}\,(\gamma-1)M^2F^2 + O(\alpha-15) \quad , \tag{3.9c}$$

$$c = \alpha^{-1}\,c_1 + \alpha^{-3}\,c_3 + \cdots \quad , \tag{3.9d}$$

where the function F(Z) is the self-similar near-wake solution found by Goldstein (1930); the constant Λ_G represents the positive displacement of the upstream boundary-layers. The three leading order solutions are then found to be

$$\Phi_0 = \Lambda_0 \quad , \tag{3.10a}$$

$$\Phi_1 = -\frac{\Lambda_0}{c_1}\,F(Z) + \Lambda_1\,Z + \Lambda_2 \quad , \tag{3.10b}$$

$$\Phi'_2 = \left(\frac{\Lambda_0 c_3}{c_1^2} - \frac{\Lambda_2}{c_1}\right) F'(Z) + T_0^2\,\Lambda_0\,Z - \frac{\Lambda_1}{c_1}\,(\,Z\,F'(Z) - F(Z)\,) \quad . \tag{3.10c}$$

where Λ_1 , Λ_2 are constants to be determined from matching. Note that the solutions above reflect the

fact that we are considering mode I waves. With (3.10a-c) at hand, it is fairly straight-forward to match with the outer solutions as $|Z| \to \infty$ and $|\xi| \to 0$ respectively. This implies that $A_1 = 0$ and yields the two required algebraic equations:

$$A_2 + B_2 = A_3 + B_3 \quad \left(= A_2 - \frac{A_0 \lambda A_G}{c_1} \right) \quad , \tag{3.11a}$$

$$A_2 + A_3 - B_2 - B_3 = \frac{2\lambda}{T_0} \left(\frac{A_0 c_3}{c_1^2} - \frac{A_2}{c_1} \right) \quad . \tag{3.11b}$$

Solution for the six unknown constants yields the second order correction to the wave-speed c to be

$$c_3 = \frac{\lambda}{2T_0 A_0} \left[\Lambda - \frac{4\pi i S(\gamma-2)}{e^2} \right] \quad . \tag{3.12}$$

In (3.12) above, Λ is a real constant which we need not give here. The imaginary part of c_3 is given by (using the definition of S)

$$c_{3i} = - \frac{2\pi(\gamma-2)\lambda^3 M^2}{e^2 \left[1 + (1/2)(\gamma-1)M^2\right]^4} \quad . \tag{3.13}$$

Since $\gamma < 2$ (in fact $\gamma = 1.4$) the imaginary part of c_3 is positive and so the flow is linearly unstable. This last remark follows from the correct identification of physically meaningful zero viscosity limit solutions of the Orr-Sommerfeld equation (cf. Lin (1955)). Another point worth noting, is that the growth rate in the hypersonic limit behaves like M^{-6} as $M \to \infty$, as opposed to the M^{-2} decay of the leading order phase-speed c_1. This means that the correction $\alpha^{-3}c_3$ always remains asymptotically smaller than $\alpha^{-1}c_1$ as the Mach number increases without bound for any functional dependence of Mach number on α.

4. Long waves, $\alpha \to 0$.

The intuitive approach to long-wavelength perturbations indicates that the exact details of the basic flow near the center-line are not that important, in obtaining leading order results at least, and the solutions depend on the basic flow characteristics at infinity. This was pointed out and utilized by Drazin and Howard (1966) in the description of several "broken-line" profiles, the results of which extend to wakes also. Originally the analysis described incompressible flows, but was later extended to include compressible ones also (Gill and Drazin (1965), Blumen et al. (1975)). The approach

essentially depends on obtaining solutions in the upper and lower half-planes respectively, and using their Wronskian to fix the eigenvalues. In the present work we present a different approach which is based on the scalings and structures of the various asymptotic regions involved. This is useful in that it motivates scalings for low-frequency/long-wavelength nonlinear stability also. The incompressible problem is described in PS1, and its low-frequency nonlinear stability analysis is given in PS2. The asymptotic limit $\alpha \to 0$ is therefore considered and as in Section 3 we choose to work with equation (2.5) for the perturbation normal velocity. Physically, we are considering instability scales that are long compared to the wake thickness but still short compared to the plate length. Further more mode I disturbances are considered since they generally provide higher growth rates (see earlier comments).

A region $Y = O(1)$ is considered first (region I), where the appropriate expansions are found to be :

$$\phi = \phi_0 + \alpha^{1/2}\phi_1 + \alpha\phi_2 + \alpha^{3/2}\phi_3 + \alpha^2\phi_4 + \cdots \quad , \tag{4.1a}$$

$$c = c_0 + \alpha^{1/2}c_1 + \alpha c_2 + \cdots \quad . \tag{4.1b}$$

The function G that appears in (2.5) also expands as follows :

$$G = G_0 + \alpha^{1/2}G_1 + \cdots \quad ,$$

where

$$G_0 = \overline{T}(Y) - M^2(\overline{u}-c_0)^2 \quad . \tag{4.1c}$$

Let us now define the following linear operator L :

$$L(.) = (\overline{u}-c_0)\frac{d(.)}{dY} - \overline{u}'(.) \quad . \tag{4.2}$$

Substitution of (4.1a-c) into (2.5) gives the following four leading order problems :

$$\frac{d}{dY}\left[\frac{1}{G_0}L(\phi_0)\right] = 0 \quad , \tag{4.3a}$$

$$\frac{d}{dY}\left[\frac{1}{G_0}\left(L(\phi_1)-c_1\phi'_0\right)\right] = 0 \quad , \tag{4.3b}$$

$$\frac{d}{dY}\left[\frac{1}{G_0}\left(L(\phi_2)-c_1\phi'_1-c_2\phi'_0\right)\right] = 0 \quad , \tag{4.3c}$$

$$\frac{d}{dY}\left[\frac{1}{G_0}\left(L(\phi_3)-c_1\phi'_2-c_2\phi'_1-c_3\phi'_0\right)\right]=0 \quad , \tag{4.3d}$$

$$\frac{d}{dY}\left[\frac{1}{G_0}\left(L(\phi_4)-c_1\phi'_3-c_2\phi'_2-c_3\phi'_1-c_4\phi'_0\right)\right]=\frac{(\bar{u}-c_0)}{\bar{T}}\,\phi_0 \quad . \tag{4.3e}$$

The appropriate solution of (4.3a) that is both even and bounded for large Y is the displacement solution

$$\phi_0 = A_0(\bar{u}-c_0) \quad , \tag{4.4}$$

and to ensure decay to zero at infinity the leading order wave-speed is

$$c_0 = 1 \quad .$$

It is not surprising to find, therefore, that long-waves are almost neutral and have phase-speeds approximately equal to that of the free-stream. Next we find

$$\phi_1 = -\,c_1A_0 \quad , \quad \phi_2 = -\,c_2A_0 \quad , \quad \phi_3 = -\,c_3A_0 \quad .$$

Substitution of (4.4) into (4.3e) gives the following solution for ϕ_4 :

$$\phi_4 = A_0(\bar{u}-1)\int_0^{\infty}\frac{G_0(y_1)\,dy_1}{(\bar{u}-1)^2}\int_{\infty}^{y_2}\frac{(\bar{u}-1)^2\,dy_2}{\bar{T}} + d_4(\bar{u}-1)\int_0^{Y}\frac{G_0(y_1)\,dy_1}{(\bar{u}-1)^2} - c_4A_0 \quad , \tag{4.5}$$

where d_4 is given by

$$d_4 = A_0\int_0^{\infty}\frac{(\bar{u}-1)^2}{\bar{T}}dY \quad , \tag{4.6}$$

since mode I disturbances are being analyzed and so $\phi prim_4(0) = 0$. It is the boundary condition (4.6) that provides the solution for the eigenvalue c_1 when the solutions are extended out to the far-field potential regions.

Inspection suggests that the solution (4.6) diverges as Y becomes large. The precise rate of divergence depends on the asymptotic behavior of the basic flow $\bar{u}$. For Blasius flow this it is given by $\bar{u} \sim 1 - (A/|Y|)e^{-Y^2}$ as $|Y| \to \infty$, while for the far wake we have $\bar{u} \sim 1 - (1/x^{1/2})e^{-Y^2}$. It can be anticipated from the results of Gill and Drazin (1965), however, that the exact asymptotic behavior is not important and the same final result is obtained to order $\alpha^{1/2}$ in the wave-speed at least. In order to illustrate the method, therefore, we choose a model asymptotic behavior at infinity. The reason for this

is that the level where the expansion breaks down can be found explicitly in terms of α (see below) and the analysis is greatly reduced. The Blasius flow gives a breakdown at a logarithmically large distance away, together with the need of a logarithmically thin region there. The analysis bears a lot of resemblance to the hypersonic limit work of Cowley and Hall (1989) on the stability of compressible boundary layers. The final result is unaltered, however, and for brevity we take a model asymptotic behavior. The far-wake profile can be worked out explicitly also (it is a simple analogue of our suggested asymptotic behavior); assume, therefore that $\bar{u} \sim 1 - qe^{-r|Y|}$ as $|Y| \to \infty$. Then the third and fourth terms in the expansion (4.1a) become comparable when $Y \sim -(1/2r)\ln(\alpha)$ due to the exponential growth of ϕ_4. A new region, II say, is introduced given by

$$Y_{II} = -\frac{1}{2r}\ln\alpha + \bar{Y} \quad ,$$

where $\bar{Y}$ is of order one. Consideration of the solution in region I for large Y suggests the following expansions in II :

$$\phi_{II} = \alpha^{1/2}\bar{\phi}_1 + \alpha\bar{\phi}_2 + \alpha^{3/2}\bar{\phi}_3 + \cdots + \alpha^{5/2}\ln\alpha\,(\hat{\phi}_1 + \hat{\phi}_2 + \ldots) + \cdots \quad . \tag{4.6}$$

These expansions are substituted into the Rayleigh equation (2.5), together with the appropriately expanded forms of G and $\bar{T}$ to give the following solutions (the solutions given here have already been matched to those in region I)

$$\bar{\phi}_1 = A_0(-qe^{-r\bar{Y}} - c_1) \quad , \tag{4.7a}$$

$$\bar{\phi}_2 = -\,c_2 A_0 \quad , \tag{4.7b}$$

$$\bar{\phi}_3 = d_4\,(-qe^{-r\bar{Y}} - c_1)\int^{\bar{Y}} \frac{dY}{(qe^{-r\bar{Y}} + c_1)^2} - c_3\,A_0 \quad , \tag{4.7c}$$

$$\hat{\phi}_1 = (-qe^{-r\bar{Y}} - c_1)\,\frac{A_0}{4r^2} \quad . \tag{4.7d}$$

To complete the solution a potential region III say, of extent α^{-1} ia also required, so introduce a new variable $Y = \alpha^{-1}\,\zeta$ with ζ order one. Consideration of (4.7a-d) as $\bar{Y} \to \infty$ implies the following expansions in III :

$$\phi_{III} = \alpha^{1/2}\Phi_0 + \alpha\Phi_1 + \alpha^{3/2}\Phi_2 + \cdots + e^{-\alpha^{-1}r\zeta}(\bar{\Phi}_0 + \alpha^{1/2}\,\bar{\Phi}_1 + \ldots) + \cdots \quad . \tag{4.8}$$

The leading order solution is

$$\Phi_0 = Be^{-\zeta} \quad , \tag{4.9}$$

where B is a constant. The final result is obtained by matching (4.9), for small ζ, with (4.7a-d) for large $\bar{Y}$. We find

$$d_4 = - A_0 c_1^2 \quad ,$$

which when coupled with the expression (4.6) for d_4 yields

$$c_1 = \pm \left[\int_0^\infty \frac{(\bar{u}-1)^2}{\bar{T}} dY \right]^{1/2} \quad . \tag{4.8}$$

This result is in complete agreement with that of Gill and Drazin (1965) and it has been shown that long-wave disturbances are almost neutral, travel with the free-stream and have growth rates of order $\alpha^{1/2}$. In view of the dependence of $\bar{T}$ on Mach number, the wake is more stable the hotter it is, i.e. the higher tha Mach number. Even though the growth rates are small with respect to the free-stream, they become leading order effects in a frame of reference that travels with unit speed and so a classical weakly nonlinear approach is not likely to work (see PS2). The situation in the hypersonic limit seems different, however, since the growth rate decays to zero like M^{-2} now.

5. Numerical solutions.

The previous sections presented some aspects of the analytical properties of the instability in the special cases of short- and long-waves. As shown the growth rates are asymptotically small and in order to find the maximally growing wavelengths or frequencies, as the case may be, the problem must be addressed numerically in a systematic search of eigenvalues. The central element of our computations is the use of correct mean-flow profiles in the calculation of stability characteristics. Particularly, this becomes essential in the near-wake where the use of model, e.g. gaussian profiles, is not appropriate. The steady equations (2.3) together with (2.3BC) are solved numerically by marching forward in x (Smith (1974), Cebeci et al. (1979), PS1). Some results for $\bar{u}$ and $\bar{T}$ are shown in Figures 1 and 2. Refinement checks were made to ensure numerical accuracy. Typically 600 points are used, 300 in the Goldstein layer and 300 in the boundary layer. Solutions are depicted at various increasing streamwise locations ranging from $\xi = 0.2$ to 2.0 (i.e. the x variation is from 0.008 to 8.0), and due to symmetry the region $y \geq 0$ alone is shown. At the smallest value of ξ the profile contains the Goldstein double-

structure quite clearly, the main part of the flow being the displaced Blasius solution. Further downstream the center-line velocity increases and the profile develops into its far-wake form which is a gaussian perturbation from the uniform flow at infinity. The center-line temperature, on the other hand, decreases as the distance from the trailing edge increases with a return to the ambient temperature at downstream infinity. The present work concentrates on the stability of the near-wake region where the initial growth of disturbances takes place. It seems likely that further downstream the wake dynamics become nonlinear as has been observed in experimental work on incompressible wakes (Sato and Kuriki (1960)).

The computational strategy is as follows. A streamwise station, ξ, is chosen and the corresponding steady-state velocity and temperature profiles are obtained. This mean flow is then used in a quasi-parallel manner (essentially ξ is a parameter) to define the compressible Rayleigh problem (2.4), (2.4BC). For a given Mach number (2.4) is integrated by starting at a large value of Y (usually the outer limit of the mean-flow calculation) where the eigenfunction is generated by its exponentially small behavior - this is readily found from (2.4) and the decaying solution is chosen in order to satisfy boundedness at infinity (the possibility of neutral oscillatory solutions as the ones found in shear layers, do not arise in the present problem; see later). A fourth order Runge-Kutta integration extends the solution to $Y = 0$, where the choice of either mode I or mode II disturbances fixes a linear eigenvalue problem which is solved by a root-finding routine. Most of the calculations address spatial stability whereby the frequency $\omega = \alpha c$ is taken to be real and the eigenvalues α and c are generally complex. This stability problem corresponds to disturbances growing or decaying with downstream distance and seems to be more relevant that the temporal problem where disturbances grow in time at fixed positions (see later discussion on convective and absolute instability). Neutral eigensolutions are also constructed, and as has been shown by Lees and Lin (1946) these have wave-speeds equal to the value of the mean flow at the generalized inflection points. If these points are denoted by Y_c, then they are given by the zeros of

$$L(Y) = \frac{d}{dY}\left[\frac{\bar{u}_Y}{\bar{T}^2}\right] \quad .$$

Non-singular neutral eigensolutions have wave-speeds equal to $\bar{u}(Y_c)$. In this case the Rayleigh equation has a removable singularity at Y_c and in computing neutral eigensolutions we used deformation of

the integration into the complex plane below the singularity. By numerical evaluation of L(Y) it can be concluded that the wake-flows under consideration have two generalized inflection points which are symmetrically placed about the wake center-line. This situation persists at arbitrarily large Mach numbers also, even though Y_c now gets pushed towards the outer edges of the wake. In Figure 3 we show a collection of L(Y) at different increasing Mach numbers and for the half-space $Y \geq 0$; the profile used is at $\xi = 0.8$ but the behavior is qualitatively the same at other wake-stations also. This in turn means that, for a given x-station and Mach number, all neutral waves have the same wave-speed.

6. Results and discussion.

Before the presentation of stability results it is useful to consider the physical nature of the possible modes. A lot of information can be found by consideration of the eigenfunctions at infinity. Our discussion follows the classification of instability waves in shear layers by Jackson and Grosch (1989). The condition imposed on the disturbance is that it remains bounded as $Y \rightarrow \infty$. For large Y, therefore, (2.4) gives the following behavior for 2D disturbances (3D ones form a simple extension, and we only want to illustrate things here) :

$$p \sim e^{\pm \alpha \Delta Y} \quad , \quad \Delta^2 = 1 - (1-c)^2 M^2 \quad . \tag{6.1}$$

The zeros of of Δ define the sonic lines where the disturbance at infinity neither grows nor decays. These are given by

$$c_{\pm} = 1 \pm \frac{1}{M} \quad .$$

It can be seen from this equation that the two sonic lines do not cross for any Mach number, and further more c_+ represents a wave with speed higher than the free-stream value and is therefore precluded on physical grounds. If Δ^2 is positive, the negative sign in the exponential in (6.1) is taken and the disturbance vanishes at infinity - the perturbation is termed subsonic since it has characteristics similar to those of incompressible stability. If Δ^2 is negative, however, the solutions are oscillatory at infinity where they take the form of outgoing or incoming waves. Such neutral waves are singular in that they do not satisfy the Lees and Lin regularity condition, but they are physically relevant as zero viscosity limit solutions of the "Orr-Sommerfeld" problem (Lees and Lin (1946), Jackson and Grosch (1989)). In the present wake problem the possibility of Δ^2 being negative does not arise, and to see

this we construct the neutral wave-speed from the Lees and Lin generalized inflection point criterion and plot it together with the equation of the sonic line c_-. A typical situation is depicted in Figure 4 for two wake stations $\xi = 0.1$ and $\xi = 1.2$. The conclusion is, therefore, that subsonic boundary conditions at infinity are adequate.

As mentioned earlier, we chose to carry out a spatial stability analysis which is, in general, more pertinent to wake-flows than a temporal one. Before presenting results it is worth mentioning that the accuracy of computed eigenvalues was checked by doubling the number of points in the mean-flow computation. The finding is that the representation of the mean-flow by 600 points produces more than graphical accuracy in the results.

First we address the convective/absolute instability question. In Figure 5a we show a collection of mode I spatial stability curves depicting the variation of $-\alpha_i$ (the spatial growth-rate) with frequency ω, and for the basic flow profiles at the streamwise locations $\xi = 0.8$, 0.6 , 0.4 , 0.2 , 0.08 , 0.06 , 0.04 , 0.02 , 0.01. The Mach number is 0.1 and the corresponding wave-number curves (α_r vs ω) are given in Figure 5b. Figure 5a shows that as we get closer to the trailing edge the maximum growth rate increases sharply and the frequency band of unstable waves decreases. This behavior is very similar to that discussed in PS1 for incompressible near-wakes. The fact that the instability is changing from convective to absolute, can be seen from Figure 5b. The curves become steeper as ξ decreases and by the stability at the final wake-station $\xi = 0.01$ is characterized by an infinite gradient. The value of $\partial\omega/\partial\alpha_r$ is tending to zero, which is the condition for absolute instability (see Huerre and Monkewitz (1985)). It is found, therefore, that there exists a region of absolute instability in the near wake for small Mach numbers; it is worth noting that the extent of this region is very small, less than $0.000001 \times L$ in dimensional terms.

The effect of Mach number on the presence of absolute instability regions is investigated next. The same wake-stations as in Figures 5 are used but the Mach number is now 3.0. Figures 6a and 6b show the variation of spatial growth-rates and wave-numbers with frequency, for the various wake-stations in question. First, note that in absolute terms the maximum growth rates decrease by more than a factor of ten and the unstable frequency band decreases by a factor of two about. In general terms, therefore, the effect of a higher Mach number is highly stabilizing (see results later also for more quantitative conclusions) The sharp features and singularity formation of Figures 5a,b are no longer present.

In fact, as Figure 6a shows, the spatial growth rate curves converge to a limiting one as ξ is decreased (the change between the curves at $\xi = 0.02$ and $\xi = 0.01$ is almost negligible). The fact that no singularity forms is clarified further by Figure 6b; the variation of α_r with frequency tends to a limiting curve with a finite slope.

The previous results addressed the effect of the basic-flow development on its stability characteristics. In what follows we pick two typical wake-stations and carry out a more detailed stability calculation. The two profiles used correspond to the values $\xi = 0.1$ and $\xi = 1.2$. They differ in that the former is a near-wake profile ($x = 0.001$) while the latter is a far-wake one ($x = 1.728$). Their respective center-line velocities are 0.0772 and 0.72. Physically the near-wake still retains many of the characteristics of the upstream boundary-layer flow while in the far-wake the double structures seen upstream are no longer present.

Figures 7a and 7b depict the effect of Mach number on the wake-stability at $\xi = 0.1$. Mode I waves are computed at Mach numbers 0, 0.5, 1, 1.5, 2, 2.5 and 3. A marked increase in stability is observed with the maximum growth rate dropping from approximately 0.27 at zero Mach number to 0.03 at a Mach number of 3. The frequency range of unstable waves also decreases. The value of the neutral wave-number (α) also decreases with Mach number as can be seen from Figure 7b; the neutral α is the value at the ends of the depicted curves since these points correspond to the almost attained neutral points on the spatial stability curves 7a. The curves go from right to left as the Mach number increases. This calculation was carried further to the higher Mach numbers of 4, 5, 6, 7, 8 and 9. The results are shown in Figures 8a and 8b. The continued increase of stability is clearly demonstrated and at a Mach number of 9 the maximum growth rate is tiny, about 0.002. Figure 8b depicts the variation of α_r with ω for the two Mach numbers of 4 and 9 only; the curves for intermediate Mach numbers are almost coincident but their end-points are at lower values of α_r. The curve for $M = 4$ is deliberately not continued to the origin since we are mainly interested at the endpoints. The conclusion that can be drawn from this calculation is that the neutral α is decreasing to zero with Mach number. The situation is quite different at a far-wake station as is shown later.

Figures 9a and 9b describe the stability characteristics of mode II waves at the station $\xi = 0.1$ and at Mach numbers of 0, 0.5 and 1.0. Comparison with Figures 7a,b shows that mode II is much more stable than mode I. For example at $M = 1$ the maximum growth rate of mode I waves is

approximately 0.15 while that for a mode II wave at the same Mach number is only 0.0025; the corresponding ranges of unstable frequencies are 0 to 0.32 and 0.006 respectively. Further more, at the wake-station under consideration, the maximum growth rate of the mode II waves increase slightly for oblique waves, but for a given Mach number they are still much lower than the corresponding 2D mode I growth rates. Figure 9b shows that the neutral wave-number is again decreasing with Mach number.

In Figures 10a and 10b we show the effect of obliqueness on the instability. In particular, mode I waves are computed at a Mach number of 3 and inclined at angles of 0, 20, 30, 45, 60 and 75 degrees respectively to the direction of the basic flow. The maximum growth rates are seen to increase as the angle increases, but the neutral frequencies decrease with angle. The final computed angle of 75 degrees has the highest maximum growth rate which is almost twice that of the 2D wave. When the angle increases further the curve begins to come down. For small wave-propagation angles the frequency where the maximum growth rate is achieved increases by a small amount from the 2D one, but when the angle increases from 60 to 75 degrees the maximum growth rate frequency shifts to a lower value. The corresponding variation of α_r with ω is shown in Figure 10b. The curves move from right to left as the angle increases.

In Figures 11a and 11b we present stability characteristics of a typical far-wake station that has $\xi = 1.2$. Mode I waves are computed and growth rate and wave-number curves are shown for the Mach numbers 0, 1, 2, 3, 4, 5, 6 and 7. The qualitative nature of the results is very similar to those of the near-wake station $\xi = 0.1$. The maximum growth rates are much lower, however (e.g. at $M = 1$ the maximum growth rates are approximately 0.018 and 0.16 respectively). The main quantitative difference between the two stations is that the neutral value of α for the far-wake profile is approaching a non-zero constant as the Mach number increases, whereas the near-wake value was decreasing to zero. This apparent difference in the physics is not too surprising in view of the completely different structure of the basic flow in the near- and far-wake respectively.

7. Conclusions.

The present study is concerned with the understanding of the physical instability mechanisms that are at play in free shear flows and in particular symmetric wakes. The main emphasis was given to the

instability of near-wakes. It was shown that these mechanisms can only be captured correctly if the correct basic flow is used. In fact our results suggest that the hypersonic limit of far-wakes is very different from that of near-wakes (this problem is currently being analyzed by the author), and the use of a model profile (e.g. gaussian distribution) in an attempt to capture the near-wake dynamics is incorrect. Using our computed basic-flow we showed that for low enough Mach numbers there exists a small region of absolute instability very near the trailing edge which disappears as the Mach number increases. The maximum spatial growth rates available increase as the trailing edge is approached, irrespective of the Mach number. Further more mode I waves are the most dangerous in the near-wake and the instability (maximum growth-rate) can be almost doubled if the wave is three-dimensional. If a temporal theory is carried out instead, some different behavior results. For example, as Chen et al. (1989) report, a far-wake profile modeled by the gaussian distribution $\bar{u} = 1 - 0.692e^{-0.69315Y^2}$ together with the corresponding temperature variation, gives the highest temporal growth rate for mode I waves which are two dimensional, and at all Mach numbers. In Figure 12 we show the spatial stability of this profile, which shows that the growth rate is larger for 3D waves inclined at an angle of about 60 degrees. Such discrepancies between spatial and temporal calculations can, therefore, be very misleading in practical applications.

ACKNOWLEDGEMNETS.

The author also wishes to thank Prof. F. T. Smith for many useful discussions. T. L. Jackson and M. Macaraeg are also thanked for many interesting comments.

REFERENCES.

Blumen, W., Drazin, P.G. and Billings, D.F. 1975 *J.Fluid Mech*, vol.71, part 2, 305-316.

Chen, J.H., Cantwell, B.J. and Mansour, N.N. 1989 *AIAA Paper*, submitted.

Cebeci, T., Thiele, F., Williams, P.G. and Stewartson, K. 1979 *Numerical Heat Transfer*, vol.2,35-60.

Cowley, S. and Hall, P. 1989 *ICASE Report No. 88-72*, and submitted *J.Fluid Mech.*

Drazin, P.G. and Howard, L.N. 1966 *Adv.Appl.Mech.*, vol.9, 1-89.

Drazin, P.G. and Reid, W.H. 1981 Hydrodynamic stability. Cambridge University Press.

Gaster, M. 1968 *Phys. Fluids*, vol.11, 723-727.

Gill, A.E. and Drazin, P.G. 1965 *J.Fluid Mech.*, vol.22, part 2, p.415.

Goldstein, S. 1930 *Proc.Camb.Phil.Soc*, vol.26, 1-30.

Gropengiesser, H. 1969 *NASA TT F-12*, 786.

Hollingdale, S.H. 1940 *Phil. Mag. (7)*, vol.29, 209-257.

Huerre, P. 1987 *Proceedings of the International Workshop on Instabilities and Non-Equilibrium Structures*, 16-21 December 1985, Valparaiso, Chile, edited by E.Tirapegui and D.Villarroel (Reidel, Dordrecht, The Netherlands, 1987), 141-177.

Huerre, P. and Monkewitz P.A. 1985 *J.Fluid Mech.*, vol.159, 151-168.

Hultgren, L.S. and Aggarwal, A.K. 1987 *Phys. Fluids*, vol.30(11), 3383-7.

Jackson, T.L. and Grosch, C.E. 1989a J.Fluid Mech., in the press.

Jackson, T.L. and Grosch, C.E. 1989b *ICASE Report No. 89-32*, and submitted to *J.Fluid Mech.*

Kumar, A., Bushnell, D.M. and Hussaini, M.Y. 1987 *AIAA Paper*, No.87-1882.

Lees, L. and Lin, C.C. 1946 *NACA Tech. Note* 1115.

Lin, C.C. 1955 The Theory of Hydrodynamic Stability, Cambridge University Press.

McKoen, C.H. 1957 *Aero. Res. Coun., Lond., Rep.* 303.

Mattingly, G.E. and Criminale, W.O. 1972 *J.Fluid Mech.*, vol.51, 233-272.

Papageorgiou, D.T. 1989 FIProceedings of the ICASE/NASA Langley Workshop on Instability and Transition, May 15- June 9, 1989, edited by M.Y.Hussaini (Springer-Verlag, New York).

Papageorgiou, D.T. and Smith, F.T. 1989 *J.Fluid Mech.*, in the press.

Papageorgiou, D.T. and Smith, F.T. 1988 *Proc. Roy. Soc. Lond.*, A419, 1-28.

Ragab, S.A. and Wu, J.L. 1988 *AIAA Paper*, No.88-0038.

Sato, H. and Kuriki, K. 1961 *J.Fluid Mech.*, vol.11, 321-352.

Smith, F.T. 1974 *J. Inst. Maths Applics*, vol.13, 127-145.

Stewartson, K. 1964 The theory of Laminar Boundary Layers in Compressible Fluids, Oxford University Press.

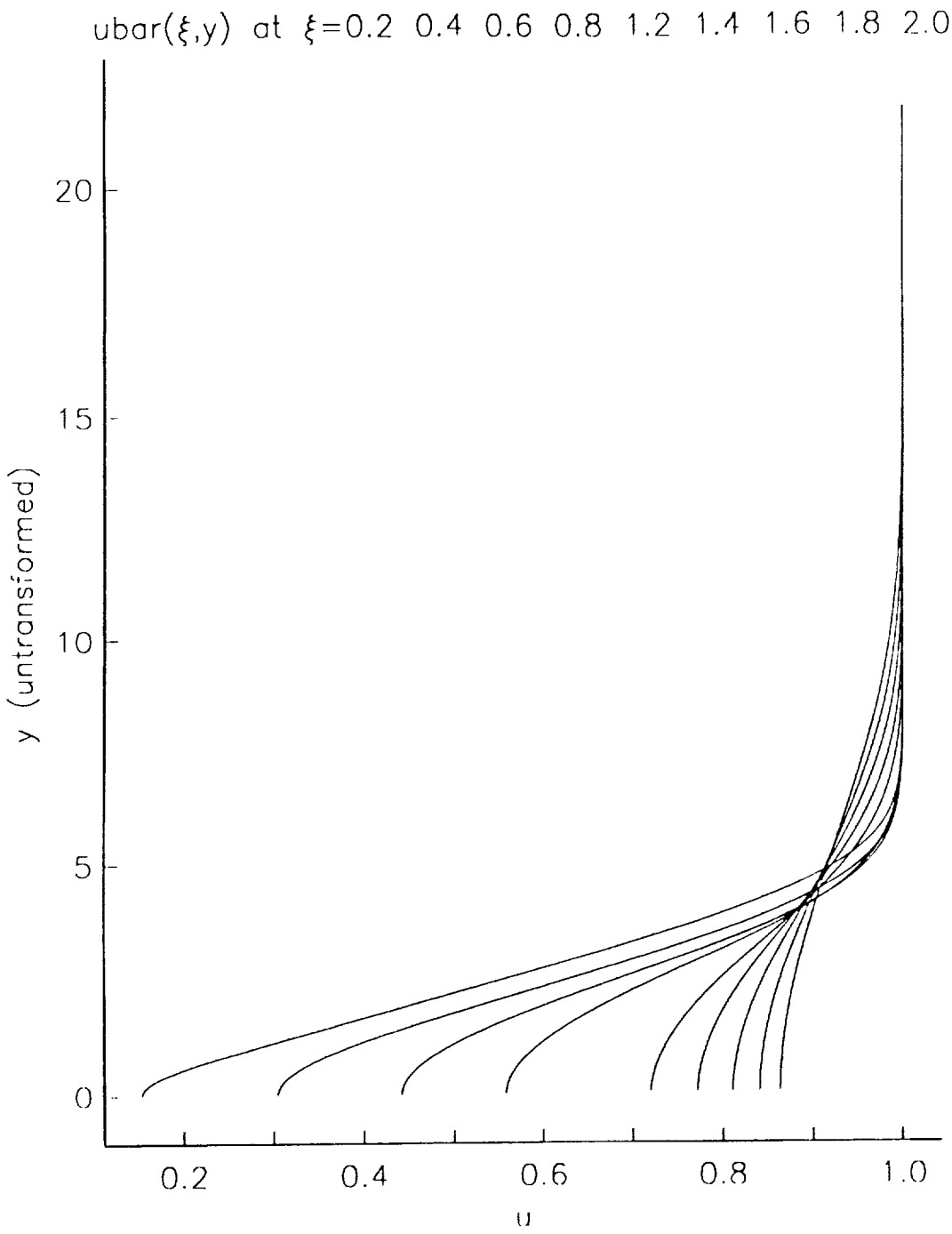

Figure 1 Streamwise development of basic flow; horizontal velocity component. Flow develops from left to right; streamwise locations are shown on the figure.

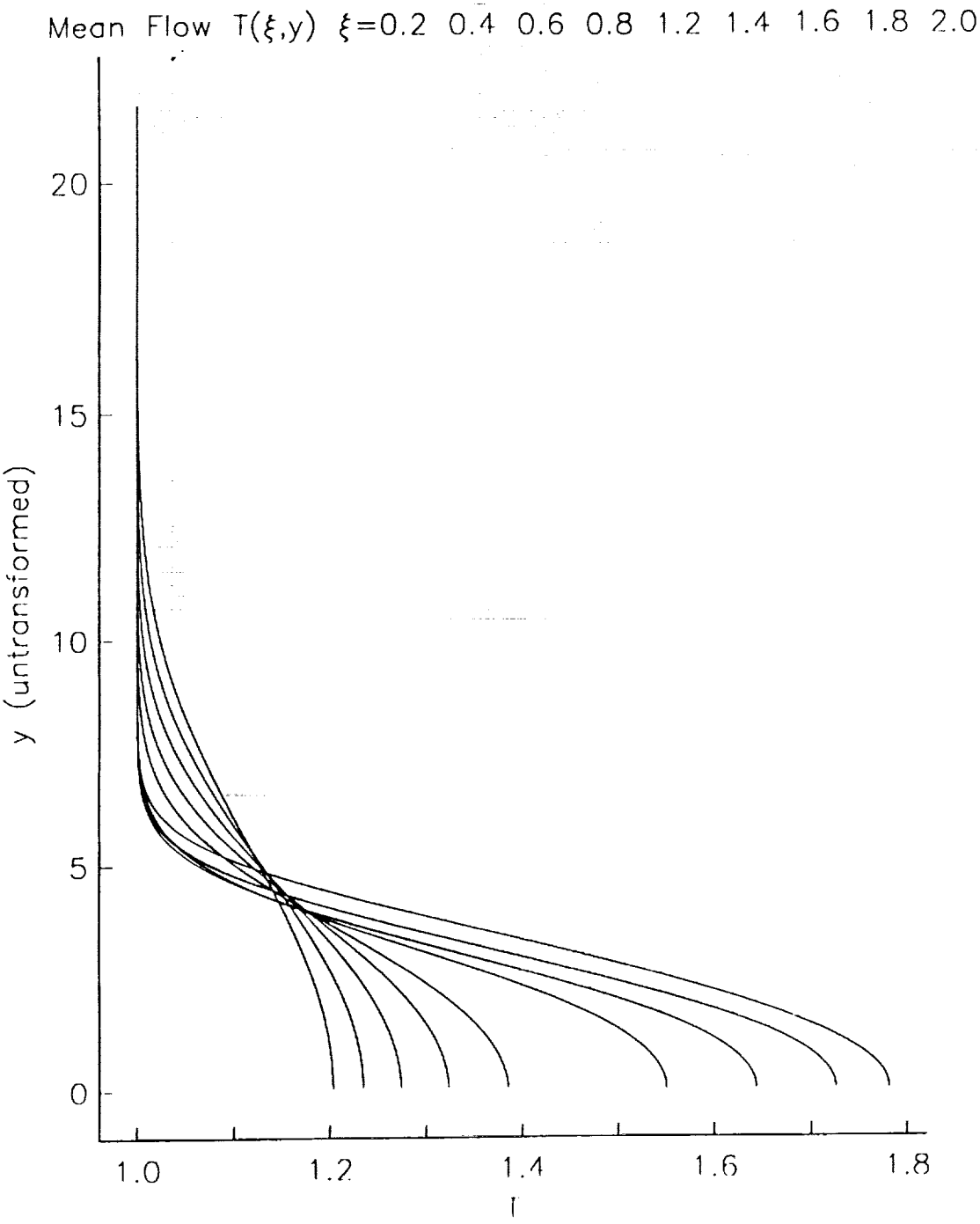

Figure 2 Streamwise development of basic flow; temperature profile. Flow develops from right to left.

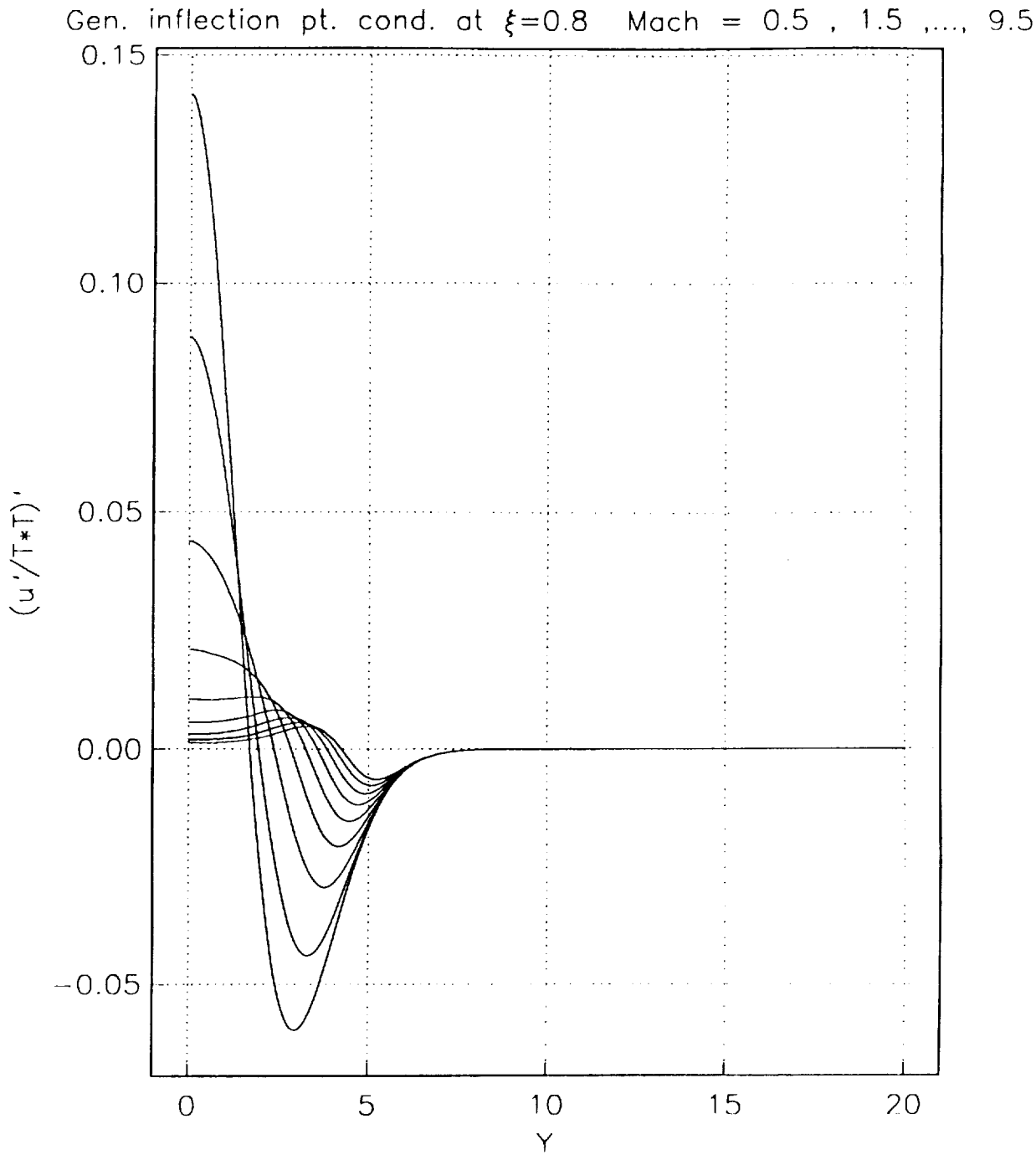

Figure 3 Generalized inflection point condition. Variation of Λ(Y) with Y. M= 0.5, 1.5, 2.5, 3.5, 4.5, 5.5, 6.5, 7.5, 8.5, 9.5. The roots of Λ move to the right with increasing Mach number.

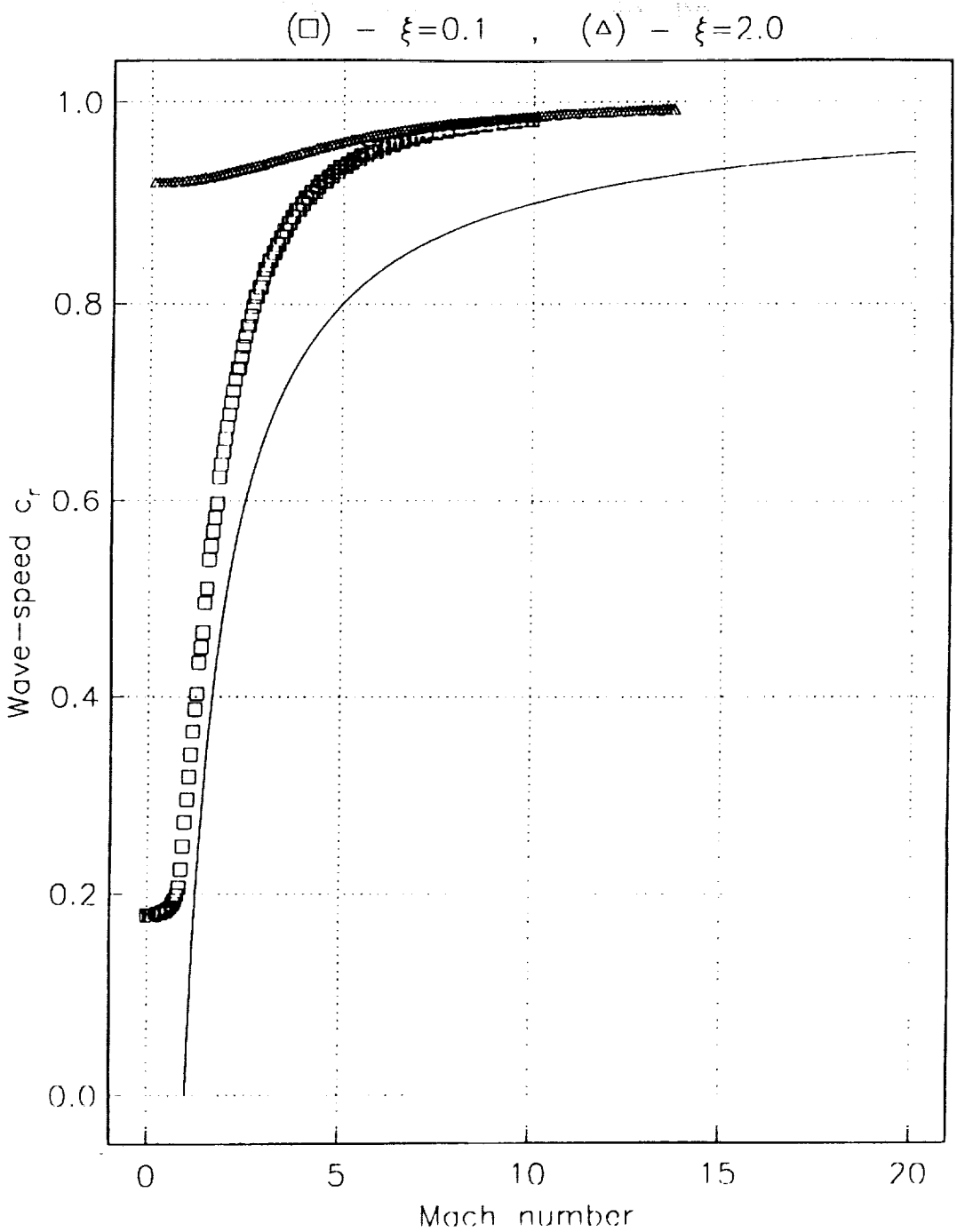

Figure 4 Mode classification diagram. Solid curve is the sonic line, the other curves show the variation of the neutral wave-speed with Mach number for the basic flow at $\xi = 0.1$ and $\xi = 1.2$.

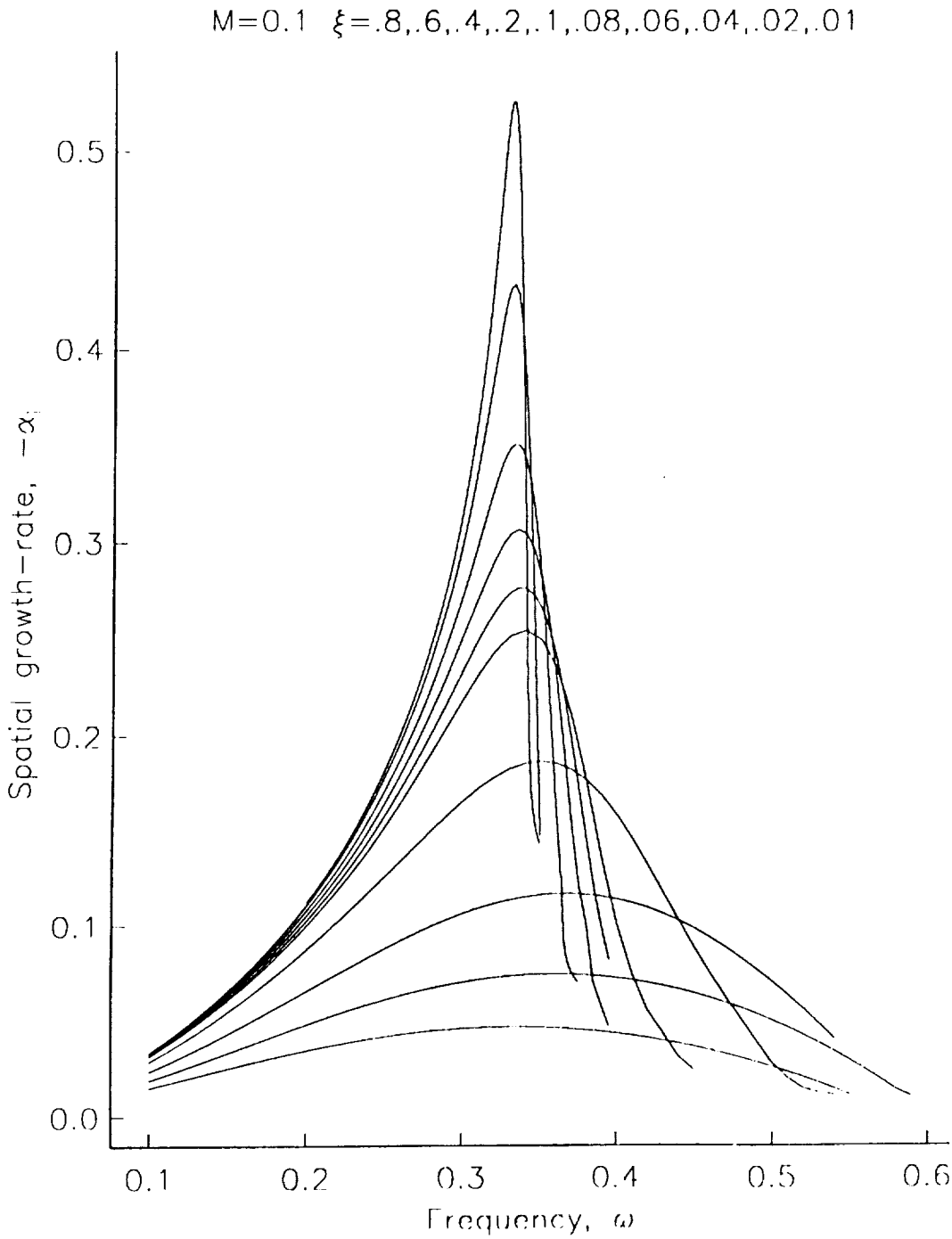

Figure 5a Spatial stability of proper compressible wake profiles at various streamwise locations. Mach number M=0.1. The graphs show the variation of the spatial growth rate $-\alpha_i$ with frequency ω. The curves correspond to the streamwise locations ξ = 0.8, 0.6, 0.4, 0.2, 0.1, 0.08, 0.06, 0.04, 0.02 and 0.01.

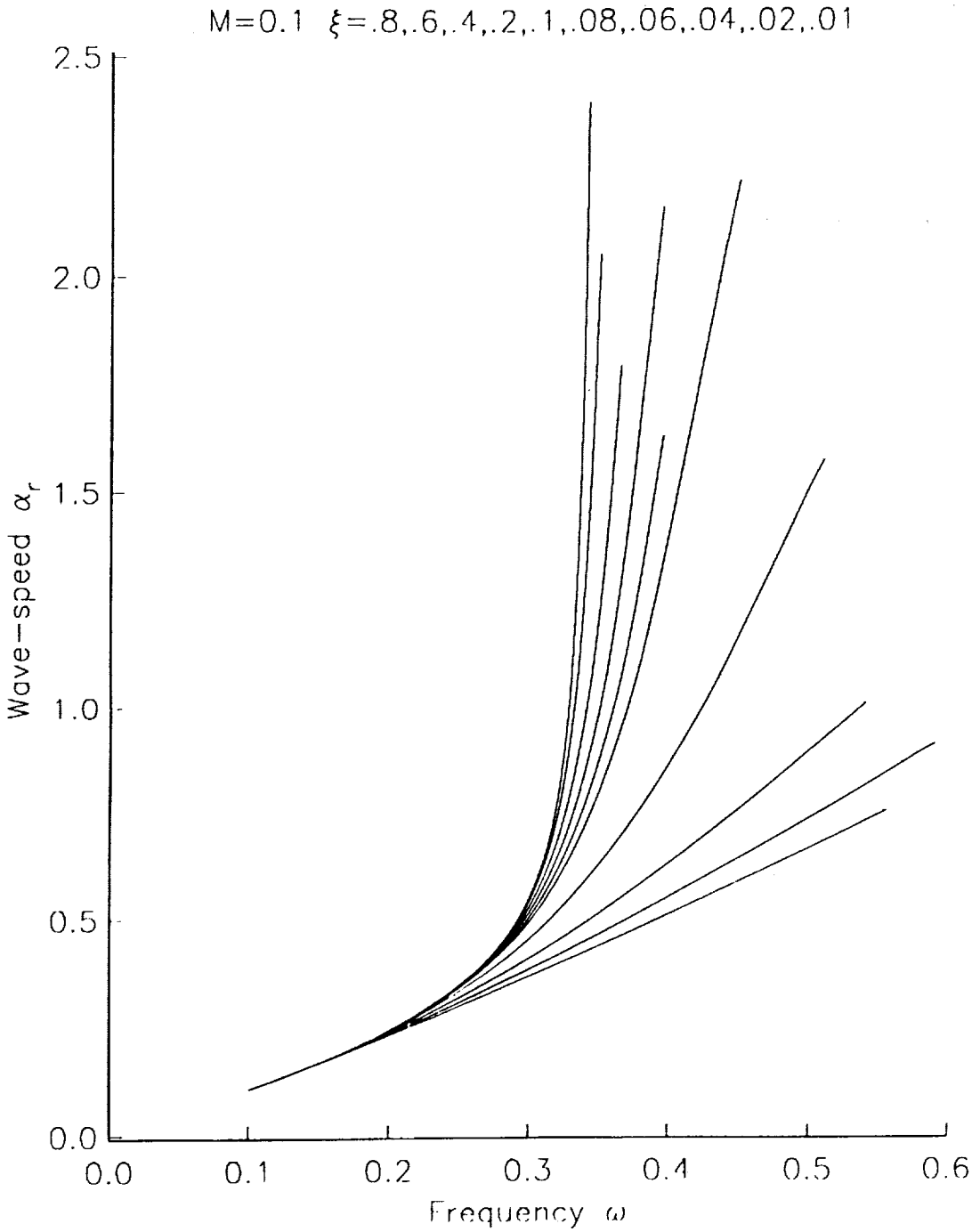

Figure 5b Same as Figure 5a but the variation of α_r with ω is now shown.

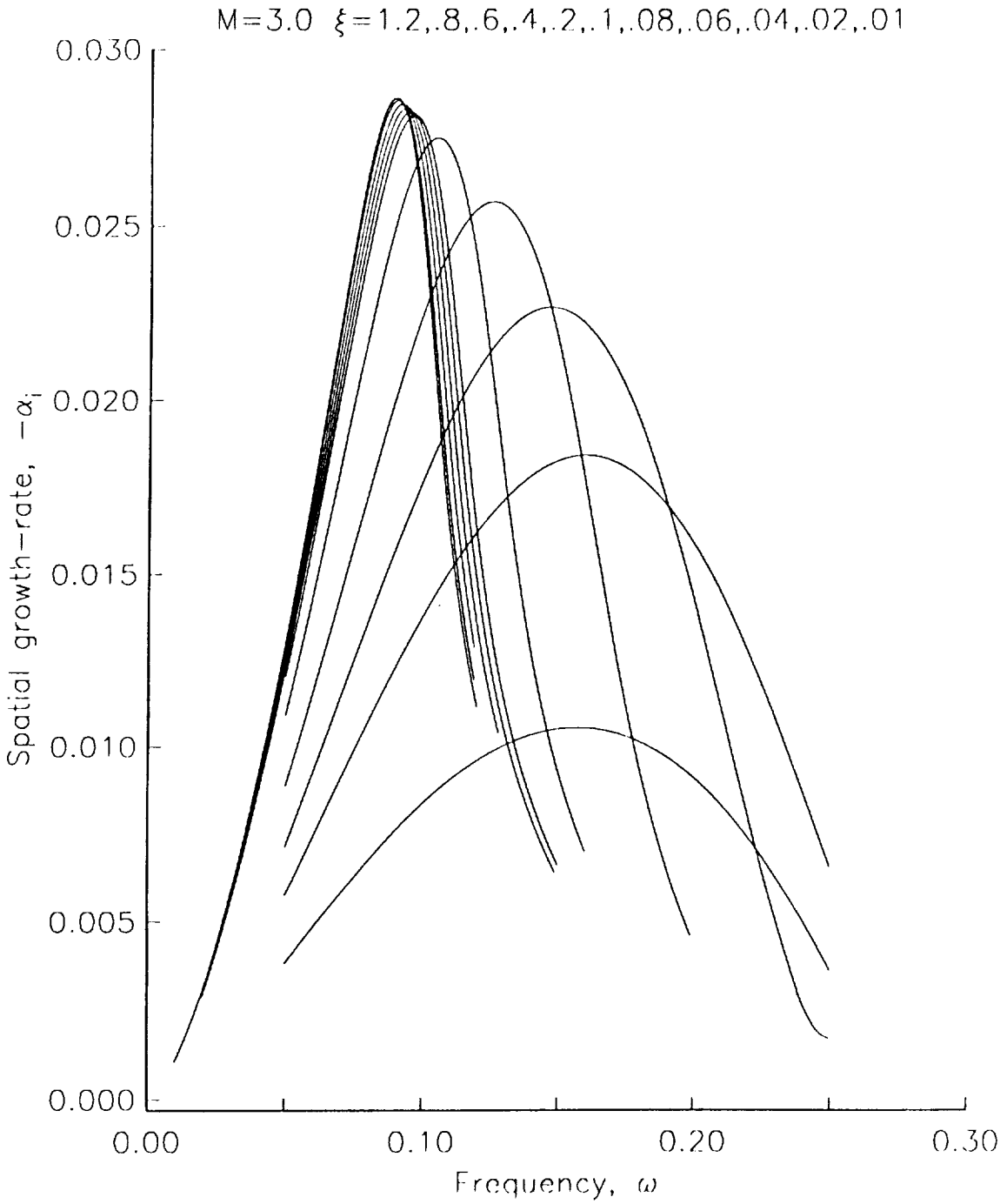

Figure 6a Spatial stability of proper compressible wake profiles at various streamwise locations. Mach number M=3.0. The graphs show the variation of the spatial growth rate $-\alpha_i$ with frequency ω. The curves correspond to the streamwise locations ξ = 0.8, 0.6, 0.4, 0.2, 0.1, 0.08, 0.06, 0.04, 0.02 and 0.01.

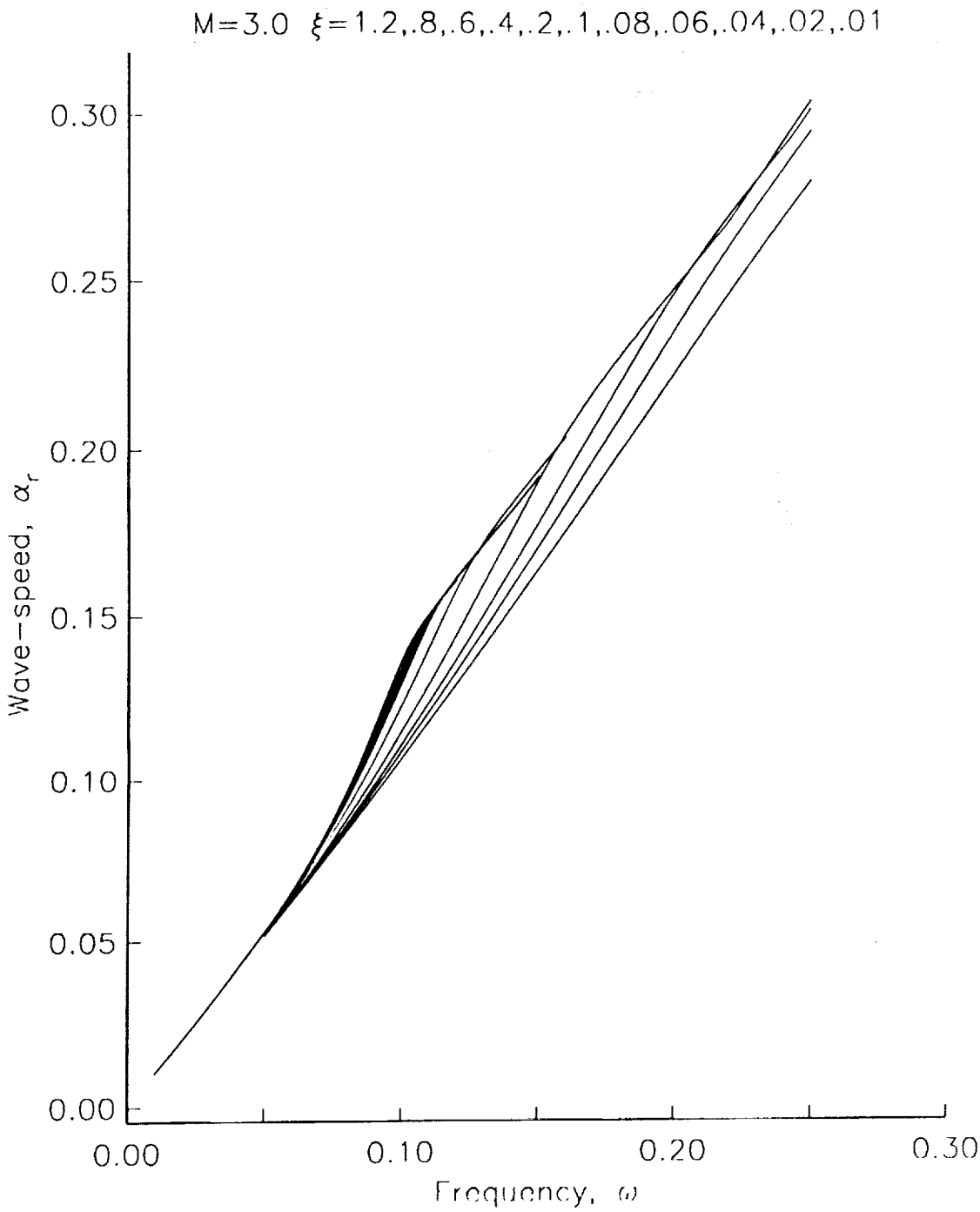

Figure 6b Same as Figure 6a but the variation of α_r with ω is now shown.

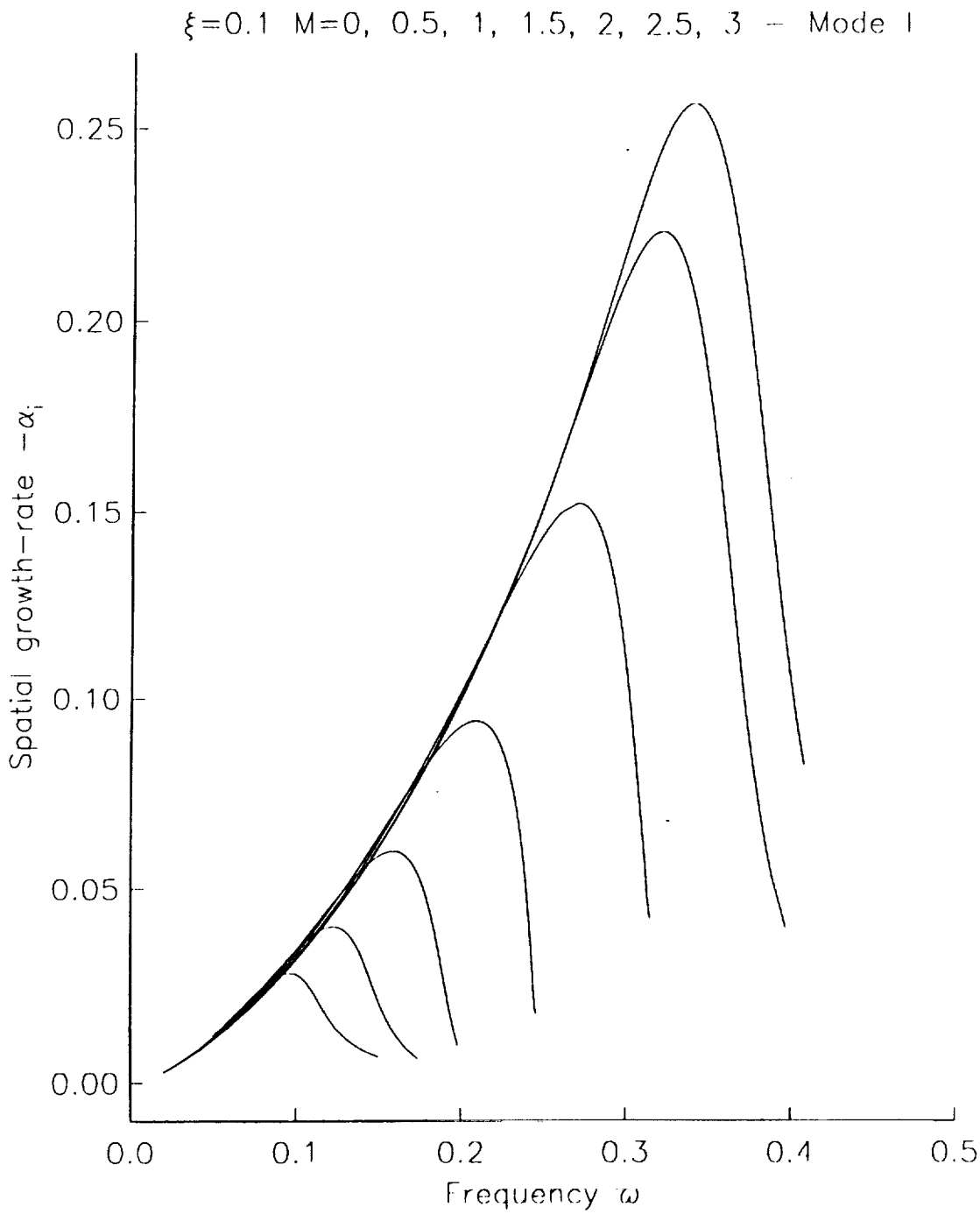

Figure 7a Near wake profile $\xi = 0.1$. Spatial growth rate curves of $-\alpha_i$ vs ω for different increasing Mach numbers M=0, 0.5, 1.0, 1.5, 2.0, 2.5, 3.0.

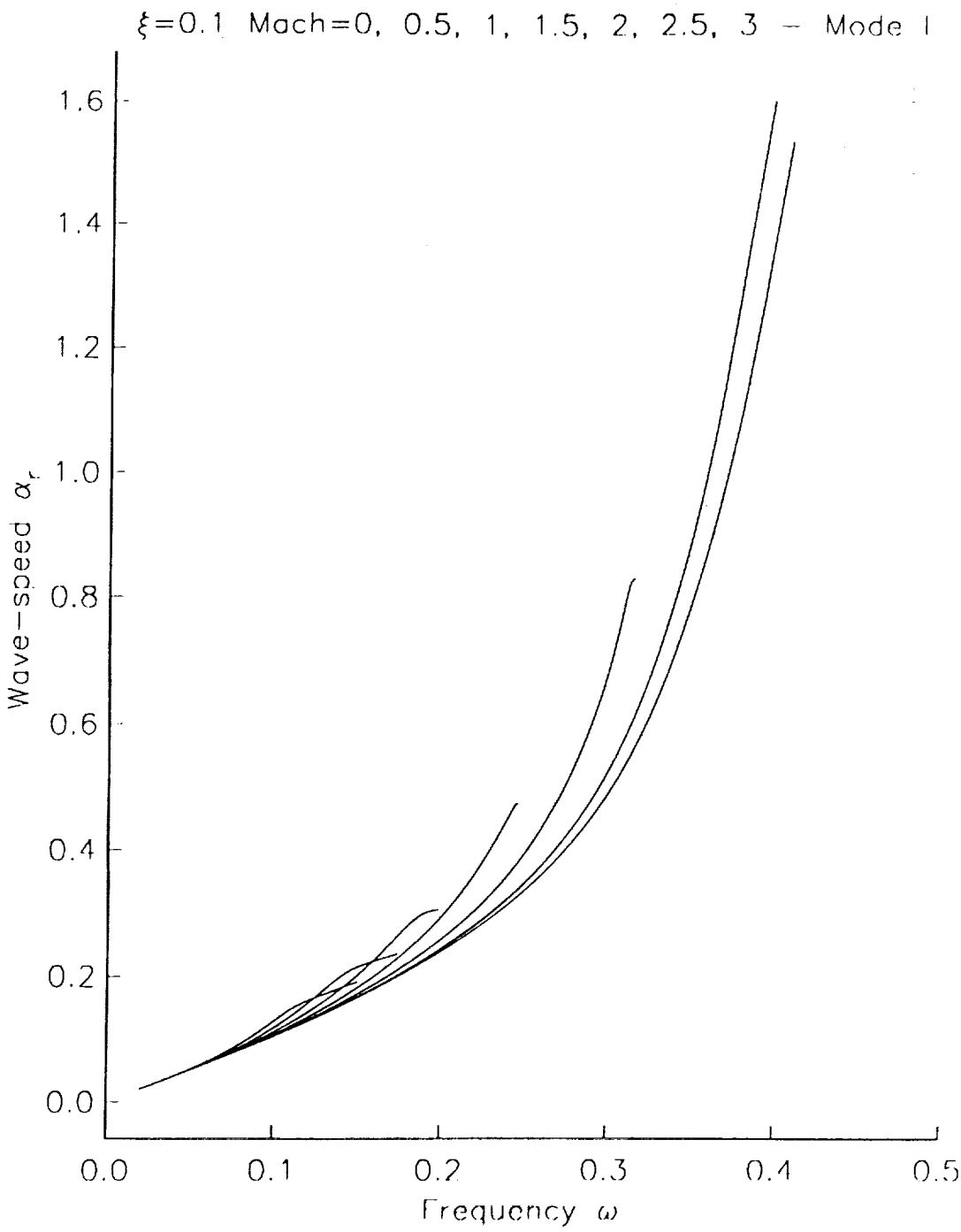

Figure 7b Same as 7a but variation of α_r with ω.

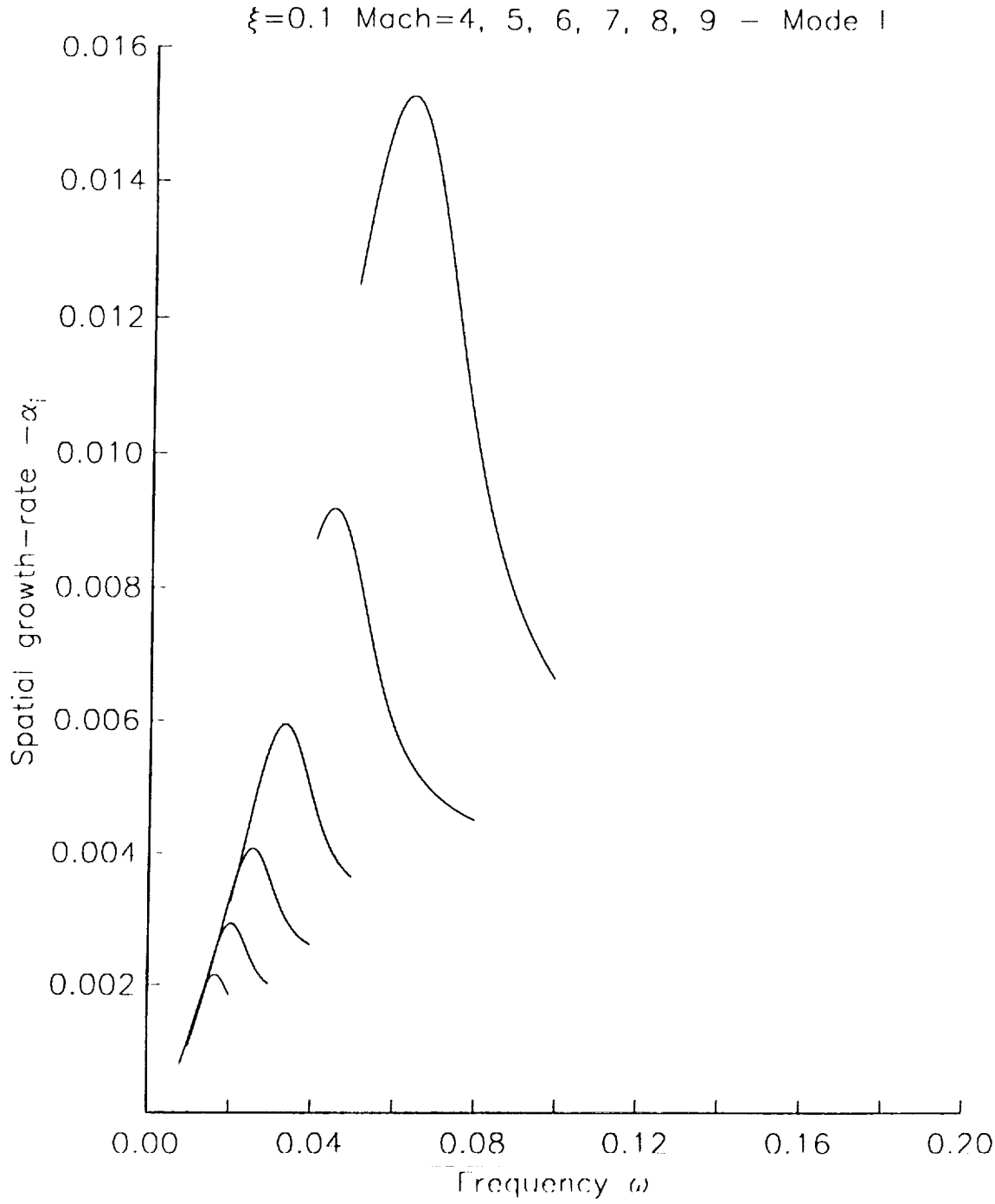

Figure 8a Near wake profile $\xi = 0.1$. Spatial growth rate curves of $-\alpha_i$ vs ω for different increasing Mach numbers M=4, 5, 6, 7, 8, 9.

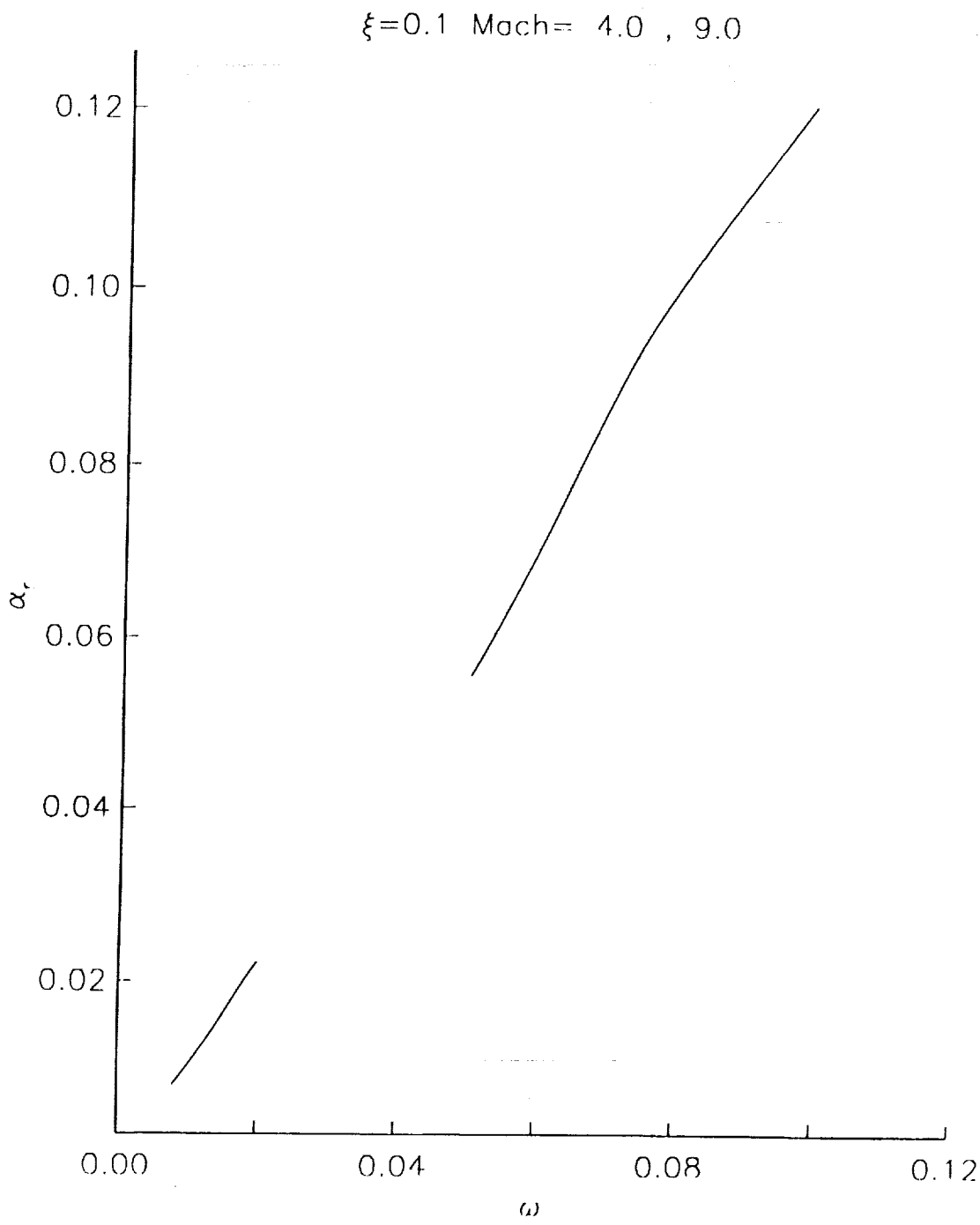

Figure 8b Near wake profile $\xi = 0.1$. Variation of α_r with ω for M=4 and 9.

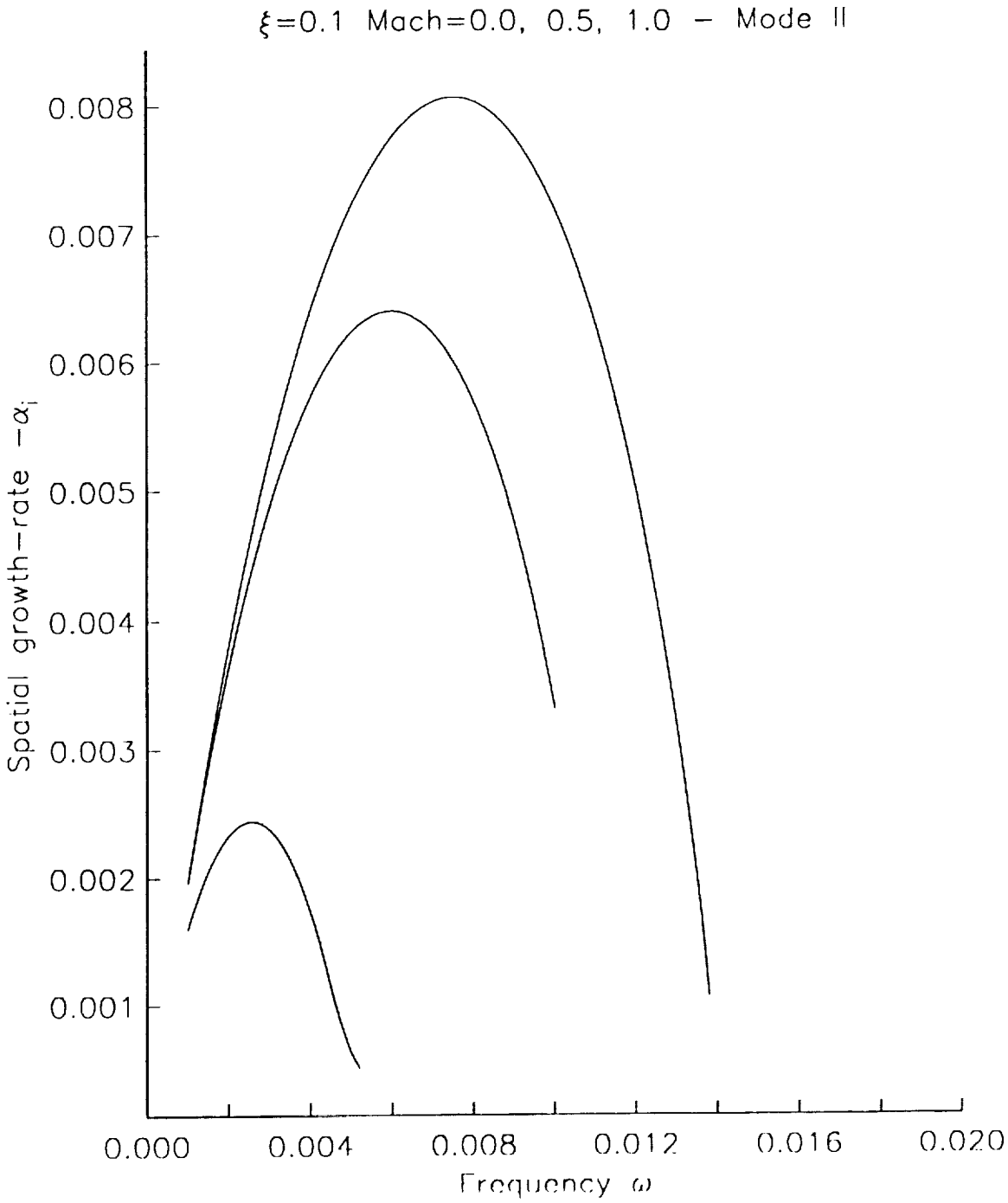

Figure 9a Near wake profile $\xi = 0.1$. Mode II waves. Spatial stability curves of $-\alpha_i$ vs ω at M=0, 0.5, 1.0.

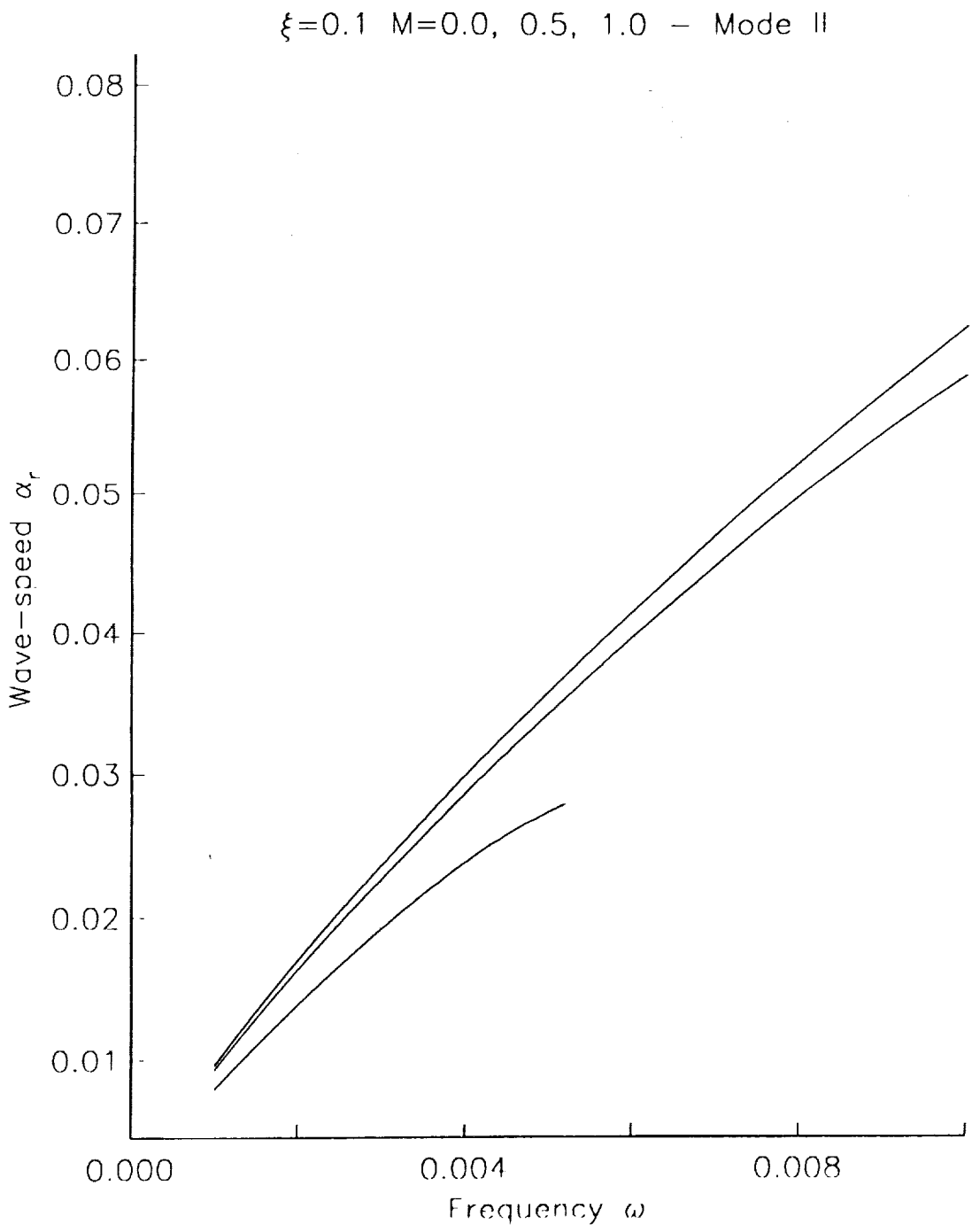

Figure 9b Near wake profile $\xi = 0.1$. Mode II waves. Spatial stability curves of α_r vs ω at M=0, 0.5, 1.0.

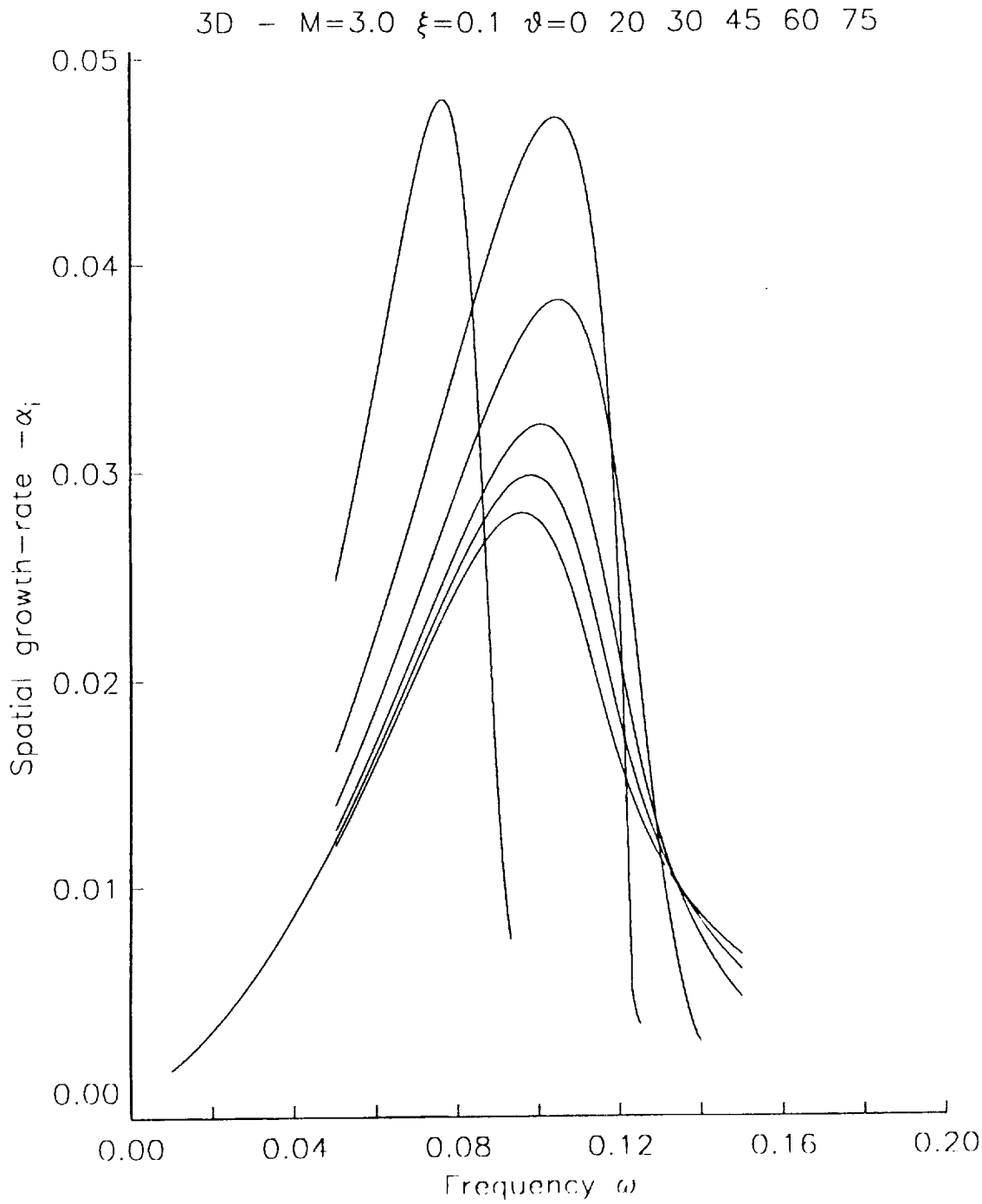

Figure 10a Near wake profile $\xi = 0.1$. 3D mode I waves. Spatial stability curves of $-\text{alpha}_i$ vs ω at a Mach number of 3.0. The angles of propagation are $\theta = 0$, 20, 30, 45, 60 and 75 degrees.

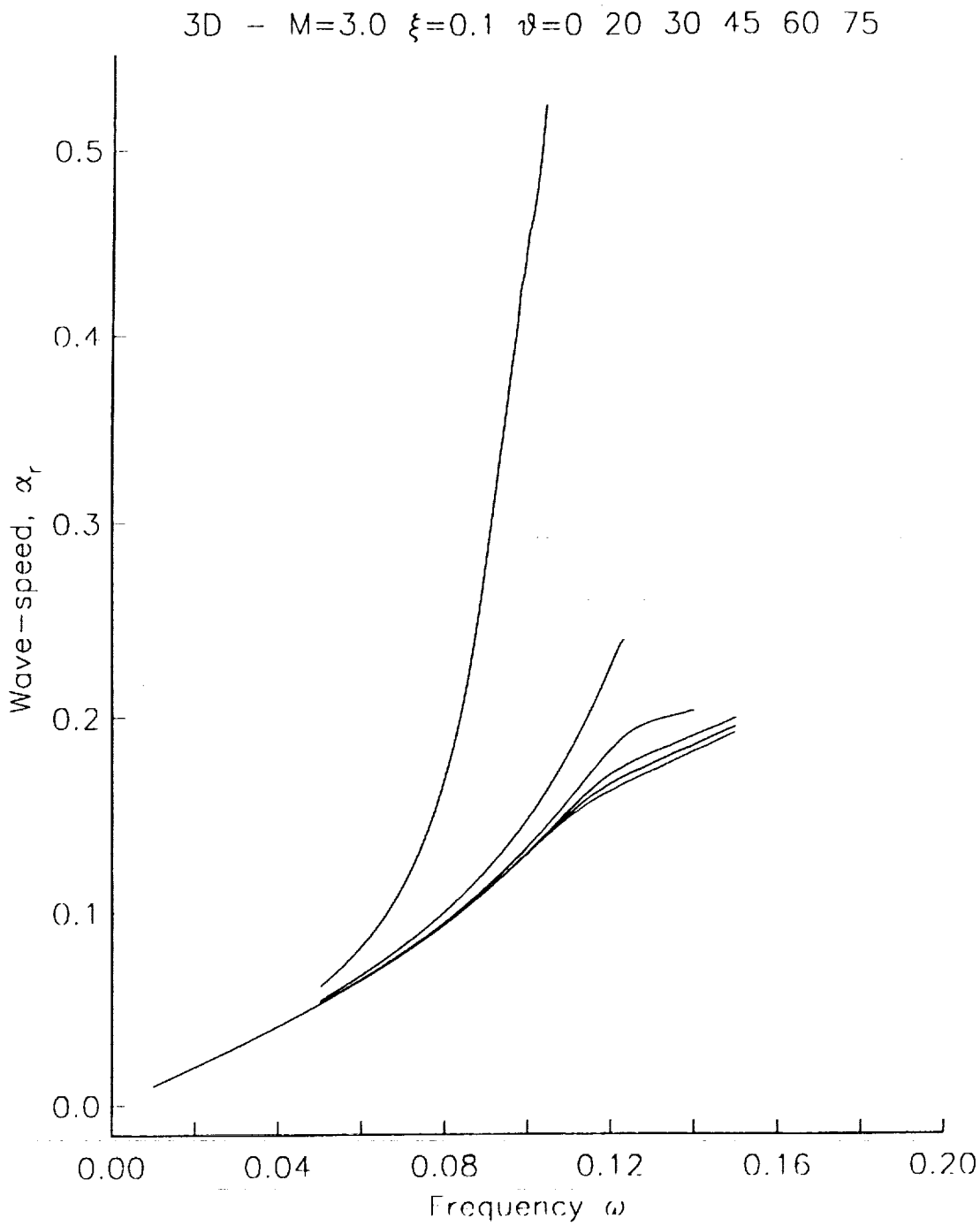

Figure 10b Same as Figure 10a but variation of α_r with ω.

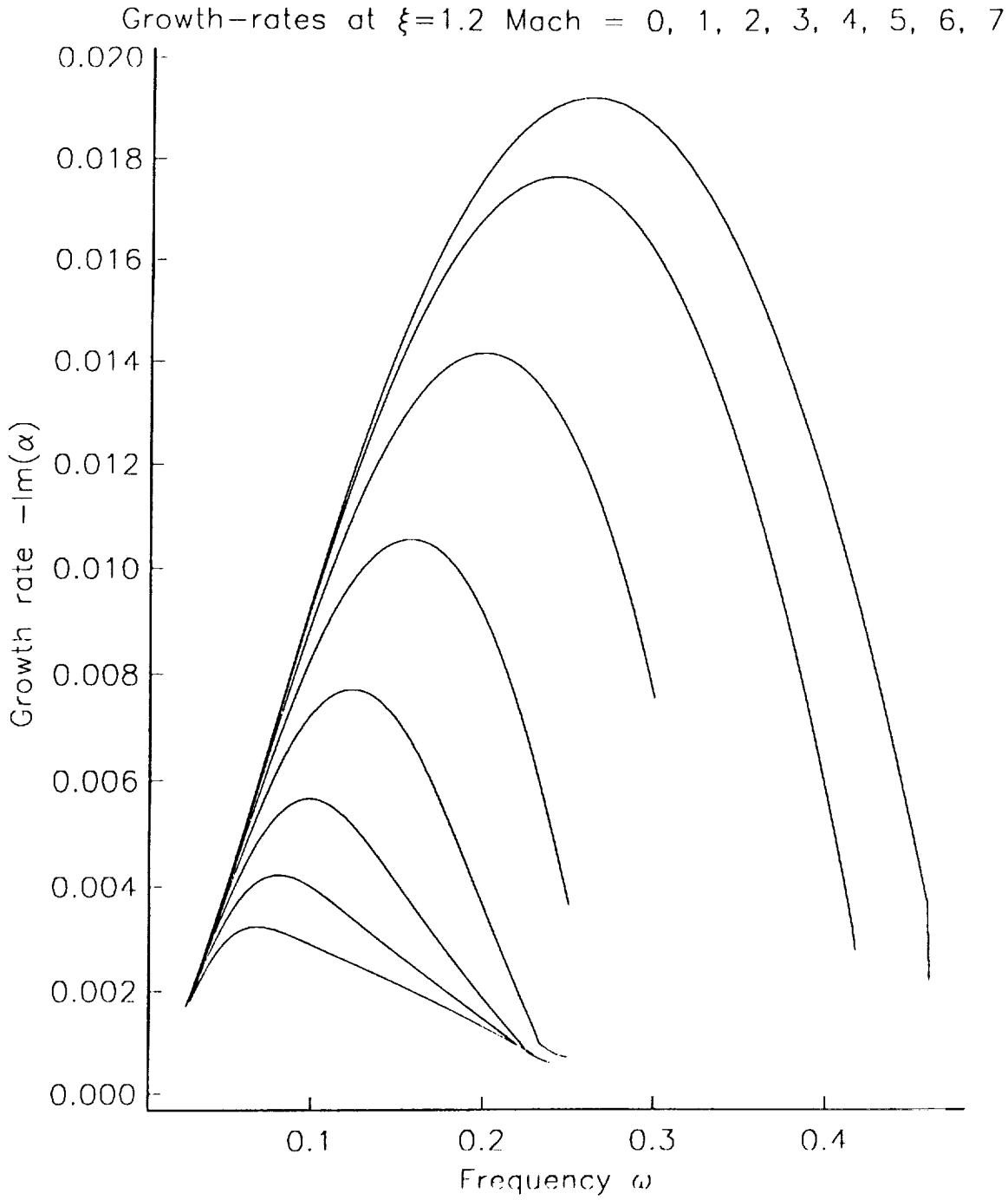

Figure 11a Far wake profile $\xi = 1.2$. Spatial stability growth rate curves of $-\text{alpha}_i$ vs ω for M=0, 1, 2, 3, 4, 5, 6 and 7.

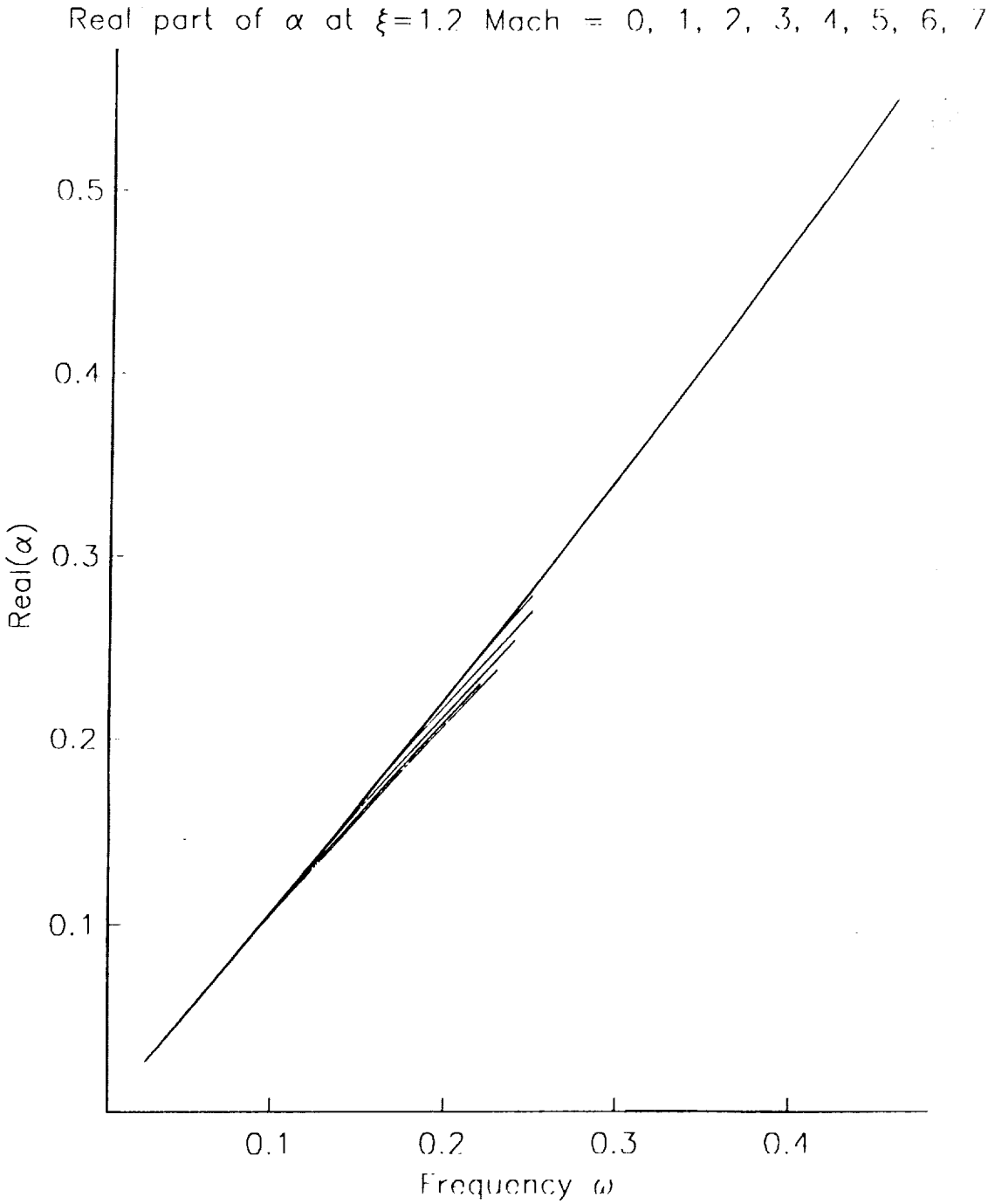

Figure 11b Same as 11a but variation of α_r with ω.

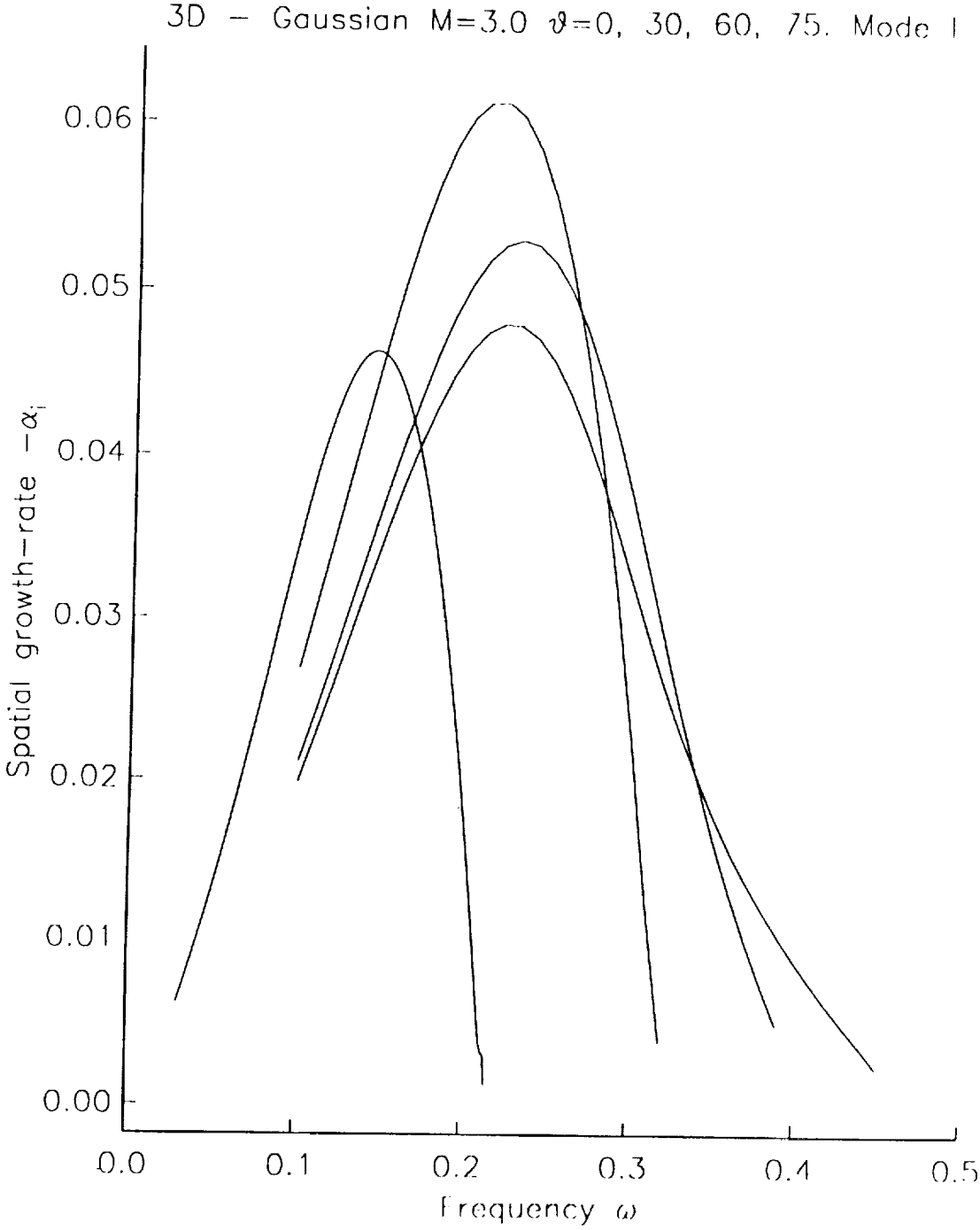

Figure 12 Gaussian model profile - 3D spatial stability at angles θ = 0, 30, 60, 75.

NASA
National Aeronautics and Space Administration

Report Documentation Page

1. Report No.	2. Government Accession No.	3. Recipient's Catalog No.
NASA CR-181911 ICASE Report No. 89-66		

4. Title and Subtitle	5. Report Date
LINEAR INSTABILITY OF SUPERSONIC PLANE WAKES	September 1989
	6. Performing Organization Code

7. Author(s)	8. Performing Organization Report No.
D. T. Papageorgiou	89-66
	10. Work Unit No.
	505-90-21-01

9. Performing Organization Name and Address	11. Contract or Grant No.
Institute for Computer Applications in Science and Engineering Mail Stop 132C, NASA Langley Research Center Hampton, VA 23665-5225	NAS1-18605
	13. Type of Report and Period Covered
12. Sponsoring Agency Name and Address National Aeronautics and Space Administration Langley Research Center Hampton, VA 23665-5225	Contractor Report
	14. Sponsoring Agency Code

15. Supplementary Notes

Langley Technical Monitor:
Richard W. Barnwell

Theoretical and Computational
Fluid Dynamics

Final Report

16. Abstract

In this paper we present a theoretical and numerical study of the growth of linear disturbances in the high-Reynolds-number and laminar compressible wake behind a flat plate which is aligned with a uniform stream. No ad hoc assumptions are made as to the nature of the undisturbed flow (in contrast to previous investigations) but instead the theory is developed rationally by use of proper wake-profiles which satisfy the steady equations of motion. The initial growth of near wake perturbation is governed by the compressible Rayleigh equation which is studied analytically for long- and short-waves. These solutions emphasize the asymptotic structures involved and provide a rational basis for a nonlinear development. The evolution of arbitrary wavelength perturbations is addressed numerically and spatial stability solutions are presented that account for the relative importance of the different physical mechanisms present, such as three-dimensionality, increasing Mach numbers enough (subsonic) Mach numbers, there exists a region of absolute instability very close to the trailing-edge with the majority of the wake being convectively unstable. At higher Mach numbers (but still not large-hypersonic) the absolute instability region seems to disappear and the maximum available growth-rates decrease considerably. Three-dimensional perturbations provide the highest spatial growth-rates.

17. Key Words (Suggested by Author(s))	18. Distribution Statement
short-, long-wave analysis, spatial stability, absolute/convective instability	02 - Aerodynamics Unclassified - Unlimited

19. Security Classif. (of this report)	20. Security Classif. (of this page)	21. No. of pages	22. Price
Unclassified	Unclassified	46	A03

NASA FORM 1626 OCT 86